2424–2441 *Nucleic Acids Research, 2020, Vol. 48, No. 5* *Published online 27 December 2019*
doi: 10.1093/nar/gkz1203

DNA binding modes influence Rap1 activity in the regulation of telomere length and MRX functions at DNA ends

Diego Bonetti, Carlo Rinaldi, Jacopo Vertemara, Marco Notaro, Paolo Pizzul, Renata Tisi, Giuseppe Zampella and Maria Pia Longhese*

Dipartimento di Biotecnologie e Bioscienze, Università degli Studi di Milano – Bicocca, 20126 Milano, Italy

Received July 26, 2019; Revised December 09, 2019; Editorial Decision December 15, 2019; Accepted December 17, 2019

ABSTRACT

The cellular response to DNA double-strand breaks (DSBs) is initiated by the Mre11–Rad50–Xrs2 (MRX) complex that has structural and catalytic functions. MRX association at DSBs is counteracted by Rif2, which is known to interact with Rap1 that binds telomeric DNA through two tandem Myb-like domains. Whether and how Rap1 acts at DSBs is unknown. Here we show that Rif2 inhibits MRX association to DSBs in a manner dependent on Rap1, which binds to DSBs and promotes Rif2 association to them. Rap1 in turn can negatively regulate MRX function at DNA ends also independently of Rif2. In fact, a characterization of Rap1 mutant variants shows that Rap1 binding to DNA through both Myb-like domains results in formation of Rap1-DNA complexes that control MRX functions at both DSBs and telomeres primarily through Rif2. By contrast, Rap1 binding to DNA through a single Myb-like domain results in formation of high stoichiometry complexes that act at DNA ends mostly in a Rif2-independent manner. Altogether these findings indicate that the DNA binding modes of Rap1 influence its functional properties, thus highlighting the structural plasticity of this protein.

INTRODUCTION

Chromosomal DNA double-strand breaks (DSBs) are highly cytotoxic lesions that can occur spontaneously during normal cell metabolism or can be induced upon exposure of cells to ionizing radiation or chemicals. Two major pathways are used for repairing DSBs: non-homologous end-joining (NHEJ), which directly religates the two broken ends (1), and homologous recombination (HR), which uses undamaged homologous duplex DNA as template for repair (2,3). HR is initiated by nucleolytic degradation (resection) of the 5′ terminated strands at both DNA ends to generate 3′-ended single-stranded DNA (ssDNA) ends that catalyze homologous pairing and strand invasion (4).

The evolutionarily conserved Mre11–Rad50–Xrs2/NBS1 complex (MRX in *Saccharomyces cerevisiae*, MRN in humans) is rapidly recruited to DSBs, where it maintains the DSB ends in close proximity, initiates DSB resection and activates the checkpoint protein kinase Tel1 (ATM in mammals) (5,6). The Mre11 subunit is a dimer that possesses both 3′-to-5′ exonuclease and ssDNA endonuclease activities (7,8). Mre11 initiates resection by catalyzing an endonucleolytic cleavage of the 5′-terminated strand at both DSB DNA ends with the support of the Sae2 protein (9–14). This MRX-mediated DNA cleavage generates an entry site for the nucleases Exo1 and Dna2, which degrade DNA in a 5′-3′ direction, coupled with Mre11 exonuclease that degrades back toward the DNA end in a 3′–5′ direction (10–14). The Rad50 subunit binds ATP and possesses ATPase activity (5,6). The characterization of Rad50 mutant variants that either stabilize or destabilize the ATP-bound conformation has shown that the ATP-bound state of MRX promotes DNA binding, end-tethering and Tel1 activation, whereas ATP hydrolysis by Rad50 leads to MRX engagement in DSB resection by allowing the access to DNA of the Mre11 nuclease active site (15,16).

Both MRX and Tel1 are also required to maintain the length of telomeres, specialized nucleoprotein complexes at the ends of eukaryotic chromosomes (17–20). MRX recruits Tel1 to both DSBs and telomeres through direct interaction between Tel1 and the Xrs2 subunit (21–24). Tel1, once loaded to DNA by the MRX complex, promotes/stabilizes MRX association to both DSBs and telomeres in a positive feedback loop (25–27). This Tel1-mediated control of MRX persistence to DNA ends is particularly important to support DNA damage resistance when MRX accumulation at DSBs is reduced, such as in the presence of the Rad50 V1269M mutation in the C-terminal ATPase domain. The *rad50-V1269M* (*rad50-VM*) allele, which was identified by

*To whom correspondence should be addressed. Tel: +39 0264483425; Fax: +39 0264483565; Email: mariapia.longhese@unimib.it

searching for *S. cerevisiae* mutants that require Tel1 to survive to genotoxic treatments (27), causes a reduction of Rad50 association at DNA ends that leads to defects in keeping the DSB ends tethered to each other (27). The lack of Tel1 exacerbates both the DNA damage hypersensitivity and the end-tethering defect of *rad50-VM* cells by further reducing the amount of $MR^{VM}X$ bound at DSBs (27). This finding suggests that this Tel1-mediated regulation of MRX retention at DNA ends is particularly important for maintaining the broken ends tethered together.

Interestingly, both the DNA damage hypersensitivity and the end-tethering defects of *rad50-VM* cells are suppressed by the lack of Rif2 (27), which acts together with Rap1 and Rif1 as negative regulator of telomere length (28). This restored DNA damage resistance and end-tethering of *rad50-VM* cells is possibly due to the lack of Rif2-mediated inhibition of MRX association at DSBs. Rif2 plays a dual function in repressing MRX retention at DNA ends. First, it decreases MRX persistence to both DSBs and telomeres in a Tel1-dependent manner (25,27). This finding, together with the observation that Rif2 competes with Tel1 for MRX interaction (25), suggests that Rif2 inhibits MRX persistence at DSBs by counteracting Tel1-mediated stabilization of MRX association at DNA ends. Second, Rif2 enhances the ATP hydrolysis activity by Rad50 (27,29), suggesting that Rif2 lowers MRX association at DNA ends by decreasing the time spent by MRX in the ATP-bound conformation that supports the DNA binding activity of the complex (15,16). Consistently with this hypothesis, *rif2Δ* cells show increased efficiency of both end-tethering and NHEJ compared to wild-type cells (27).

Rif2 directly binds to Rap1 (28,30), which is a DNA binding protein that negatively regulates telomere length, activates transcription at promoters, represses transcription at the silent mating-type loci and at telomeres, and inhibits telomeric fusions by NHEJ (31). Rap1 is essential for cell viability and its partial dysfunction can lead to loss of silencing (32–34), telomere lengthening (33,35) and telomere fusions (36,37). Rap1 consists of three conserved domains: a BRCT domain in the N-terminal region, a centrally located DNA binding domain (DBD) with two Myb-like folds, and a C-terminal domain called RCT. The RCT domain is sufficient for Rap1 interaction with Rif2 and Rif1, as well as with Sir3 and Sir4, two nucleosome-binding factors involved in gene silencing (28,38). The lack of this domain causes both an increase in telomere length that is similar to that observed when Rif1 and Rif2 are concomitantly lacking (28,39), and loss of mating-type and telomeric silencing similar to that observed when Sir3 or Sir4 is deleted (40,41).

While there are no obvious Rif2 orthologs in mammals, a Rap1 ortholog harbouring similar domain structure is present in both fission yeast and humans. However, unlike budding yeast Rap1, which directly binds to telomeric DNA, both mammalian and fission yeast Rap1 associate with telomeres through their interaction with the telomeric protein TRF2 (42). In mammals, Rap1 and TRF2 interact with TRF1, TIN2, POT1 and TPP1 to form a protein complex called shelterin that maintains telomere identity (43). While TIN2, TPP1 and POT1 have no obvious *Saccharomyces cerevisiae* orthologs, both human TRF1 and TRF2 share the DNA binding domain with *S. cerevisiae* Rap1 (43).

Crystal structures have shown that $Rap1^{DBD}$ binds telomere repeat DNA in a sequence-specific fashion through both the Myb-like motifs, which make contact with the two half-sites of a recognition sequence consisting of two direct repeats spaced by 1 or 3 bp (44–47). Immediately after the C-terminal Myb-like domain, a wrapping loop folds back and interacts with the N-terminal Myb-like motif to form a closed complex on DNA. Interestingly, Rap1 was shown to form *in vitro* higher stoichiometry complexes, where a single Myb-like domain is bound to both telomeric and non-telomeric double-stranded DNA (dsDNA) with lower affinity (48–50). This transition is thought to be due to a transient opening of the C-terminal wrapping loop that leads to a destabilization of the clamped structure (49,50).

Rap1 dysfunction was shown to cause MRX-mediated telomere degradation (51,52), suggesting that Rap1 inhibits MRX activity at least at telomeres. However, whether Rap1 exerts this function through Rif2 is unclear. On one hand, the lack of $Rap1^{RCT}$ was shown to increase the association of MRX at telomeres (51), suggesting that Rap1 acts through Rif2 to negatively regulate MRX association at telomeres. On the other hand, MRX fails to associate to long telomeric DNA sequences and this effect requires Rap1 but not Rif2 or $Rap1^{RCT}$ (53). Furthermore, artificial tethering of Rap1 molecules adjacent to non-telomeric DNA ends needs Rif2 to decrease MRX accumulation at nearby DNA ends only when Tel1 is absent (25). In any case, whether Rap1 represses MRX association at DSBs is unknown.

Here we show that Rif2 counteracts MRX association to DNA ends in a manner dependent on Rap1, which binds to DSBs and promotes Rif2 association to them. In fact, *rif2* or *rap1* alleles specifically impaired in Rap1 or Rif2 interaction, respectively, suppress the DNA damage hypersensitivity and the end-tethering defect caused by the *rad50-VM* allele by increasing MRX association to DSBs. Rap1 in turn can inhibit MRX functions in a Rif2-dependent and independent manners. In fact, binding of both Rap1 Myb-like domains to DNA allows formation of Rap1-DNA complexes that act through Rif2 in the negative regulation of telomere length and MRX association at DNA ends. On the other hand, Rap1 binding to DNA through a single Myb-like domain allows formation of high stoichiometry Rap1-DNA complexes that act mostly in a Rif2-independent manner. Altogether, these findings indicate that, depending of its DNA binding mode, Rap1 can form complexes with different properties that impact on Rap1 functions *in vivo* and on its ability to interact with Rif2.

MATERIALS AND METHODS

Yeast strains and media

Strain genotypes are listed in Supplementary Table S1. Strain JKM139, used to detect protein association at DSBs, was kindly provided by J. Haber (Brandeis University, Waltham, USA). Strains JYK40.6, used to detect end-tethering, was kindly provided by D. P. Toczyski (University of California, San Francisco, USA). UCC3537 and UCC3515 strains, used to detect transcriptional silencing,

were kindly provided by D. Gottschling (Fred Hutchinson Cancer Research Center, Seattle, USA). Plasmids containing the *rap1-H709A* and *rap1-D727A* alleles were a gift from C. Wolberger (Johns Hopkins University, Baltimore, USA), while plasmids containing the *rap1-R747L* and *rap1-Y592A* alleles were generated by site-directed mutagenesis. To integrate these alleles into the genome, *RAP1* ORFs were amplified and fused by PCR to a *LEU2* marker. The resulting PCR amplification products, containing the *RAP1* coding sequence and the *LEU2* marker gene, were used to transform cells in order to replace the *RAP1* wild type sequence with the mutagenized DNA fragments.

Cells were grown in YEP medium (1% yeast extract, 2% bactopeptone) supplemented with 2% glucose (YEPD), 2% raffinose (YEPR) or 2% raffinose and 3% galactose (YEPRG). Synthetic complete (SC) medium and SC medium with 5-fluoroorotic acid (5-FOA) (1%) were used to assay *URA3* gene silencing. SC medium containing a limiting concentration of adenine (2 mg/l) was used for the colony color assay based on the *ADE2* reporter gene. Gene disruptions were generated by one-step PCR disruption method. All the experiments have been performed at 25°C.

Search for *rif2* mutations that suppress the DNA damage sensitivity of *rad50-VM* cells

To search for *rif2* alleles that suppress the *rad50-VM* sensitivity to camptothecin (CPT), genomic DNA from a strain carrying the *LEU2* gene located 245 bp downstream of the *RIF2* stop codon was used as template to amplify by low-fidelity PCR a *RIF2* region spanning from position −550 bp to +410 bp from the *RIF2* coding sequence. 30 independent PCR reaction mixtures were prepared, each containing 5U GoTaq® G2 Flexi DNA polymerase (Promega), 10 ng genomic DNA, 500 ng each primer, 0.5 mM each dNTP (dATP, dTTP, dCTP), 0.1 mM dGTP, 0.5 mM $MnCl_2$, 10 mM Tris–HCl (pH 8.3), 50 mM KCl and 3 mM $MgCl_2$. The resulting PCR amplification products, containing the *RIF2* coding sequence and the *LEU2* marker gene, were used to transform a *rad50-VM* mutant strain in order to replace the *RIF2* wild type sequence with the mutagenized DNA fragments. Transformant clones were selected on synthetic medium without leucine and then assayed by drop test for increased viability in the presence of CPT compared to *rad50-VM* cells.

Search for *rap1* mutations that suppress or exacerbate the DNA damage sensitivity of *rad50-VM* cells

To search for *rap1* alleles that suppress or exacerbate the *rad50-VM* sensitivity to CPT, genomic DNA from a strain carrying the *LEU2* gene located 350 bp upstream of the *RAP1* ATG start codon was used as template to amplify by low-fidelity PCR a *RAP1* region spanning from position −500 bp to +220 bp from the *RAP1* coding sequence. 30 independent PCR reaction mixtures were prepared, each containing 5U GoTaq® G2 Flexi DNA polymerase (Promega), 10 ng genomic DNA, 500 ng each primer, 0.5 mM each dNTP (dATP, dTTP, dCTP), 0.1 mM dGTP, 0.5 mM $MnCl_2$, 10 mM Tris–HCl (pH 8.3), 50 mM KCl and 3 mM $MgCl_2$. The resulting PCR amplification products, containing the *RAP1* coding sequence and the *LEU2* marker gene, were used to transform a *rad50-VM* mutant strain in order to replace the *RAP1* wild type sequence with the mutagenized DNA fragments. Transformant clones were selected on synthetic medium without leucine and then assayed by drop test for increased or decreased viability in the presence of CPT compared to *rad50-VM* cells.

Immunoprecipitation

Total protein extracts were prepared by breaking cells in 300 μl of buffer containing 50 mM HEPES pH 7.5, 250 mM NaCl, 20% glycerol, 1 mM sodium orthovanadate, 60 mM β-glycerophosphate, 1 mM PMSF and protease inhibitor cocktail (Roche Diagnostics). An equal volume of phosphate buffer containing 250 mM NaCl was added to clarified protein extracts and tubes were incubated for 2 h at 4°C with 50 μl of a 50% (v/v) Protein A-Sepharose together with anti-Rap1 polyclonal antibodies (gift from D. Shore, University of Geneva, Switzerland). The resins were then washed twice with 1 ml of phosphate buffer containing 250 mM NaCl. Bound proteins were visualized by western blotting with anti-Rap1 or anti-Myc (9E10) antibodies after electrophoresis on a 10% SDS-polyacrylamide gel.

ChIP and qPCR

ChIP analysis was performed with anti-Myc (9E10), anti-HA (12CA5) and anti-Rap1 antibodies, as previously described (27). Quantification of immunoprecipitated DNA was achieved by quantitative real-time PCR (qPCR) on a Bio-Rad MiniOpticon apparatus. Triplicate samples in 20 μl reaction mixture containing 10 ng of template DNA, 300 nM for each primer, 2× SsoFast™ EvaGreen® supermix (Bio-Rad #1725201) (2× reaction buffer with dNTPs, Sso7d-fusion polymerase, $MgCl_2$, EvaGreen dye, and stabilizers) were run in white 48-well PCR plates Multiplate™ (Bio-Rad #MLL4851). The qPCR program was as follows: step 1, 98°C for 2 min; step 2, 98°C for 5 s; step 3, 60°C for 10 s; step 4, return to step 2 and repeat 30 times. At the end of the cycling program, a melting program (from 65°C to 95°C with a 0.5°C increment every 5 s) was run to test the specificity of each qPCR. Data are expressed as fold enrichment at the HO-induced DSB over that at the non-cleaved *ARO1* locus, after normalization of each ChIP signal to the corresponding input for each time point. Fold enrichment was then normalized to the efficiency of DSB induction. Rif2 and Rap1 binding was also detected at six different Y'-containing telomeres (6Y') (54). Data are expressed as fold enrichment at 6Y' over that at the non-telomeric *ARO1* locus, after normalization of each ChIP signal to the corresponding input.

Southern blot analysis of telomere length

To determine the length of native telomeres, XhoI-digested genomic DNA was subjected to 0.8% agarose gel electrophoresis and hybridized with a ^{32}P-labeled poly(GT) probe. Standard hybridization conditions were used.

DBD expression and purification

The coding region of Rap1 or Rap1^{P520L} DNA binding domain (residues 358-601) was cloned into pET21a bacterial expression vector at EcoRI and XhoI restriction sites. Recombinant proteins were produced in Lennox medium (LM) (10 g/l tryptone, 5 g/l yeast extract, 5 g/l NaCl) with addition of 100 mg/l ampicillin. Cultures were grown in LM at 37°C until OD_{600} ∼0.6-0.8 and induced with 10 mM isopropylthiogalactoside at 20°C for 18 h. Proteins were extracted and purified from the soluble fractions by immobilized-metal affinity chromatography on nickel-nitrilotriacetic acid agarose (Jena Bioscience, Jena, Germany) as previously described (55). Elution fractions containing highest protein concentrations were buffer exchanged by gel filtration chromatography on PD10 (GE Healthcare, Little Chalfont, UK) against 10 mM sodium phosphate buffer pH 7.0. Protein concentration was determined by Bradford protein assay (Bio-Rad), using bovine serum albumin as standard. SDS-PAGE was performed on 14% SDS polyacrylamide gel and stained with Gel-Code Blue (Pierce, Rockford, USA) after electrophoresis.

Electrophoretic mobility shift assay (EMSA)

EMSA was performed by incubating 20 nM of 21 bp ^{32}P-labeled dsDNA (5′-CCGCACACCCACACACCAGT G-3′) with purified Rap1^{DBD} (from 20 nM to 120 nM) at room temperature for 15 min in binding buffer (20 mM HEPES–KOH pH 7.6, 10% v/v glycerol, 100 mM KCl, 0.1 mM EDTA, 1 mM DTT, 25 μg/ml BSA) to a final volume of 20 μl. Reactions were loaded on a 6% acrylamide/bisacrylamide 0.5× TBE gel and separated by running for 2 h at 150 V. Gels were soaked for 15 min in 10% methanol, 10% acetic acid solution, vacuum-dried and exposed to an autoradiography film.

Model construction

For the Rap1-Rif2 models, crystal structure of Rap1, spanning from 675 to 825 amino acids, in complex with Rif2, spanning from 64 to 388 amino acids, was retrieved from protein data bank (PDB code: 4BJ5). The loops not resolved in the PDB structure were modelled with Prime (Schrödinger Release 2019-2: Prime, Schrödinger, LLC, New York, NY, 2019). This structure was mutated *in silico* by using the PyMOL mutagenesis tool (The PyMOL Molecular Graphics System, Version 2.0 Schrödinger, LLC) to generate Rap1-Rif2^{L341S} and Rap1^{R747L}-Rif2. For the Myb-DNA models, crystal structure of Rap1 spanning from 358 to 602 amino acids in complex with telomeric dsDNA is present in protein data bank (PDB code: 3UKG) with a level of resolution of 2.95 Å. Such X ray crystal structure was cut into two submodels: the first one includes Myb-N domain (from 358 to 446 residues) and DNA, while the second one includes Myb-C domain (from 447 to 586 residues) and DNA. These submodels were used to generate the mutant variants by performing *in silico* substitution using PyMOL. Four models were generated: DNA-Myb-N, DNA-Myb-N^{R381W}, DNA-Myb-C and DNA-Myb-C^{P520L}.

Refine of models

All models were relaxed with unbiased molecular dynamics simulation using GROMACS (56) (https://doi.org/10.1016/j.softx.2015.06.001). For each system, five replicas were performed at 300 K and 1 atm for 150 ns with an integration step of 2 fs for a total of 750 ns of simulation time. All structures were placed in a cubic box with minimum distance between atoms of the solute and box edges being 1.0 nm. Boxes were filled with CHARMM-appropriate TIP3P water molecules and electrically neutralized by adding an appropriate number of K^+ and Cl^- ions. Proper protonation state of residues was calculated at 7.0 pH. Such simulations were carried out using CHARMM36 (57) as force field that well reproduces protein and nucleic acids behavior. The concatenated trajectories were analyzed using cluster analysis in order to select the most representative conformation for each system that were used as starting point for subsequent umbrella sampling simulations.

Umbrella sampling

The simulation protocol was divided into two steps: a steered molecular dynamics (SMD) and an umbrella sampling (US) simulation. The SMD step was necessary to generate a series of configurations along the selected reaction coordinate, that is the separation event of the complexes. During this simulation, the subunits were pushed away one from the other by applying a biasing potential to their centers of mass (COMs). COMs of subunits were oriented along x-direction of cartesian space. During steering/pulling simulations, a harmonic potential of 1000 kJ/mol nm^2 was applied only along x-direction with a pull rate of 0.005 nm/ps in order to obtain a COM displacement of 5 nm in 1 ns. The x-dimension of each simulation box were enlarged by 15.0 nm respect to the previous simulations and additional K^+ and Cl^- ions were added to obtain an ionic concentration of 100 mM. Frames representing a COM spacing of 0.1 nm, referred to as configurations, were extracted from pulling trajectories and were used as starting points for US simulations. US simulation was performed at 300 K and 1 atm for 20 ns for each configuration restraining it within a window corresponding to the chosen COM distance by applying harmonic potential of 1000 kJ/mol nm^2. All simulations were carried out using CHARMM36 as force field.

Potential of Mean Force (PMF) calculation

PMF was calculated from the umbrella histograms using the weighted histogram analysis method (WHAM) (58) implemented in GROMACS. For PMF calculation, the following settings have been used: 50 bins per 1 nm, 100 bootstraps to obtain an average bootstrapped PMF and error estimates. PMF was set to zero at the distance between COMs where the pull force drops to the minimum, which is 6.0 nm for Rap1-Rif2 system (Supplementary Figure S1A) and 5.5 nm for DNA-Myb systems (Supplementary Figure S1B and C). Individual umbrella histograms were weighted with estimated integrated autocorrelation times (IACTs) smoothed along the reaction coordinate (x-direction) using gaussians with standard deviation $\sigma = 0.15$ nm (59).

RESULTS

Identification of *rif2* alleles that restore DNA damage resistance of *rad50-VM* cells

The lack of Rif2 increases the association of the MRX complex at both DSBs and telomeres, and restores DNA damage resistance and end-tethering of *rad50-VM* cells (25,27). To better understand how Rif2 exerts these functions, we searched for *rif2* mutations that, similar to *RIF2* deletion, suppress the hypersensitivity to DNA damaging agents of *rad50-VM* cells. Linear *RIF2* PCR products were obtained by low-fidelity PCR and then transformed into *rad50-VM* cells in order to replace the corresponding *RIF2* wild type sequence with the mutagenized DNA fragments. As mutations in any MRX subunit (including *rad50-VM*) are particularly sensitive to camptothecin (CPT), which stabilises DNA topoisomerase I cleavage complexes that can lead to replication-dependent DSBs (60), transformant clones were screened for increased viability in the presence of CPT compared to *rad50-VM*. This screen yielded 8 *rif2* alleles increasing CPT resistance of *rad50-VM* cells (Figure 1A and B). Suppression was not specific to CPT, as all the *rif2* alleles also suppressed the sensitivity of *rad50-VM* cells to the DNA alkylating agent methyl methanesulphonate (MMS) (Figure 1A and B).

Sequence analysis revealed that three alleles contained single missense mutations either in the N-terminus (*rif2-A78D*) or in the C-terminus (*rif2-I295R* and *rif2-L341S*) of the protein (Figure 1C). One other allele had multiple missense mutations (*rif2-S170L, I348F*). The remaining four alleles had a frameshift mutation at codon 193, 294, 360 or 368 (Figure 1C), resulting in truncation of the protein past residue 194, 317, 364 or 387, respectively (with 1, 2, 3, 4 or 19 amino acids added to the end of the protein, respectively, as a result of the frameshift mutation). Similar to *rif2Δ*, all the *rif2* alleles carrying missense mutations suppressed also the DNA damage hypersensitivity of *rad50-VM tel1Δ* cells (Figure 1D), indicating that Tel1 is not required for the suppression.

Consistently with Rif2 dysfunctions, all the *rif2* mutants displayed overelongated telomeres, although to different extents. In particular, telomere length in *rif2-A78D*, *rif2-I295R*, *rif2-193FS*, *rif2-294FS*, *rif2-360FS* and *rif2-368FS* cells was similar to that of *rif2Δ* cells (Figure 1E). Tel1 was required for telomere overelongation in both *rif2Δ* and *rif2* mutants, as telomeres in *rif2Δ*, *rif2-A78D*, *rif2-S170L, I348F*, *rif2-I295R* and *rif2-L341S* cells lacking Tel1 were as short as in *tel1Δ* cells (Supplementary Figure S2). The finding that *rif2Δ*, *rif2-A78D*, *rif2-S170L, I348F*, *rif2-I295R* and *rif2-L341S* alleles restored DNA damage resistance of *rad50-VM* cells even in the absence of Tel1 (Figure 1D) suggests that telomere lengthening is not involved in the suppression mechanism.

The lack of Rif2-Rap1 interaction is sufficient to restore DNA damage resistance of *rad50-VM* cells

Rap1 directly binds Rif2 and Rif1 proteins to form a protein complex that negatively controls telomerase-mediated telomere elongation (28,35,61). A so-called 'Velcro-like' macromolecular complex was described (30), in which each Rif2 molecule binds two different Rap1 molecules through two independent interfaces: the Rif2^{AAA+} domain, formed by the three-dimensional association of the ASCE motif (residues 88–282) and an α bundle (residues 61–88 together with residues 282–371), and an N-terminal peptide, defined as RBM, comprising residues 36–48. The structure of Rap1^{RCT} domain bound to Rif2^{AAA+} and Rif2^{RBM} domains was resolved (30) (PDB code: 4BJ5) (Figure 2A) and revealed that the Rap1 F708 and P705 residues interact hydrophobically with Rif2 residues L79, F342 and V350, while Rap1 R747 forms a salt bridge with Rif2 E347. An additional minor interface is provided by the Rif2 C-terminus comprising residues 371–395 and referred to as CTD.

Although the A78D mutation is located in the Rif2 N-terminal region while I295R and L341S are located in the α helical bundle of the protein, both these two regions compose the AAA+ domain (Figure 2A). These amino acid substitutions did not impair Rif2 protein level, as protein extracts from wild type, *rif2-A78D*, *rif2-I295R* and *rif2-L341S* cells contained similar amounts of Rif2 protein (Figure 2B). Interestingly, these three mutations affect residues facing a hydrophobic pocket within Rif2^{AAA+} domain (Figure 2A), suggesting that their substitution with polar or charged residues impinges on the stability of the α helical bundle, affecting the interface of the Rif2^{AAA+} domain towards the Rap1^{RCT} domain. Furthermore, apart from the frameshift mutation in position 193 that deletes the majority of the Rif2 polypeptide, truncation of the C-terminus past residue 364 or 387 by the frameshift mutations at codons 360 and 368, respectively, causes loss of the C-terminal tail, which is involved in the generation of the interface between Rif2 and Rap1. Altogether, these findings raise the possibility that most of the identified *rif2* mutations affect the interaction between Rif2 and Rap1, suggesting that the lack of this interaction is sufficient to restore DNA damage resistance of *rad50-VM* cells.

To investigate whether the missense mutations above could impair Rap1-Rif2 interaction, we focused on Rif2 L341S by exploiting a computational approach based on biased molecular dynamics simulations (62). In detail, the simulation protocol was divided into two steps. First, a steered molecular dynamics (SMD) was performed in order to generate a series of configurations along the selected reaction coordinate, that is the separation of Rap1 and Rif2 proteins in the complex. Secondly, an actual umbrella sampling (US) simulation was performed on each single configuration obtained, in order to explore the whole trajectory of the complex dismantling. Finally, the absolute binding free energy can be deduced from the potential of mean force (PMF), which represents the free energy profile G along a given reaction coordinate ξ (63). In this case, the reaction coordinate is the separation of Rap1 and Rif2 and this allows calculating the difference in free energy within the regions of the phase space corresponding to bound and unbound states, giving an estimate of the free energy of binding (ΔG). As a control, in order to validate the dependability of the computational protocol, we tested the R747L amino acid substitution in Rap1, which is known to specifically affect the interaction between Rap1 and Rif2 (64). Consistently with a reduced Rap1^{R747L}-Rif2 interaction, the US simulation revealed a significant ΔG increase in the

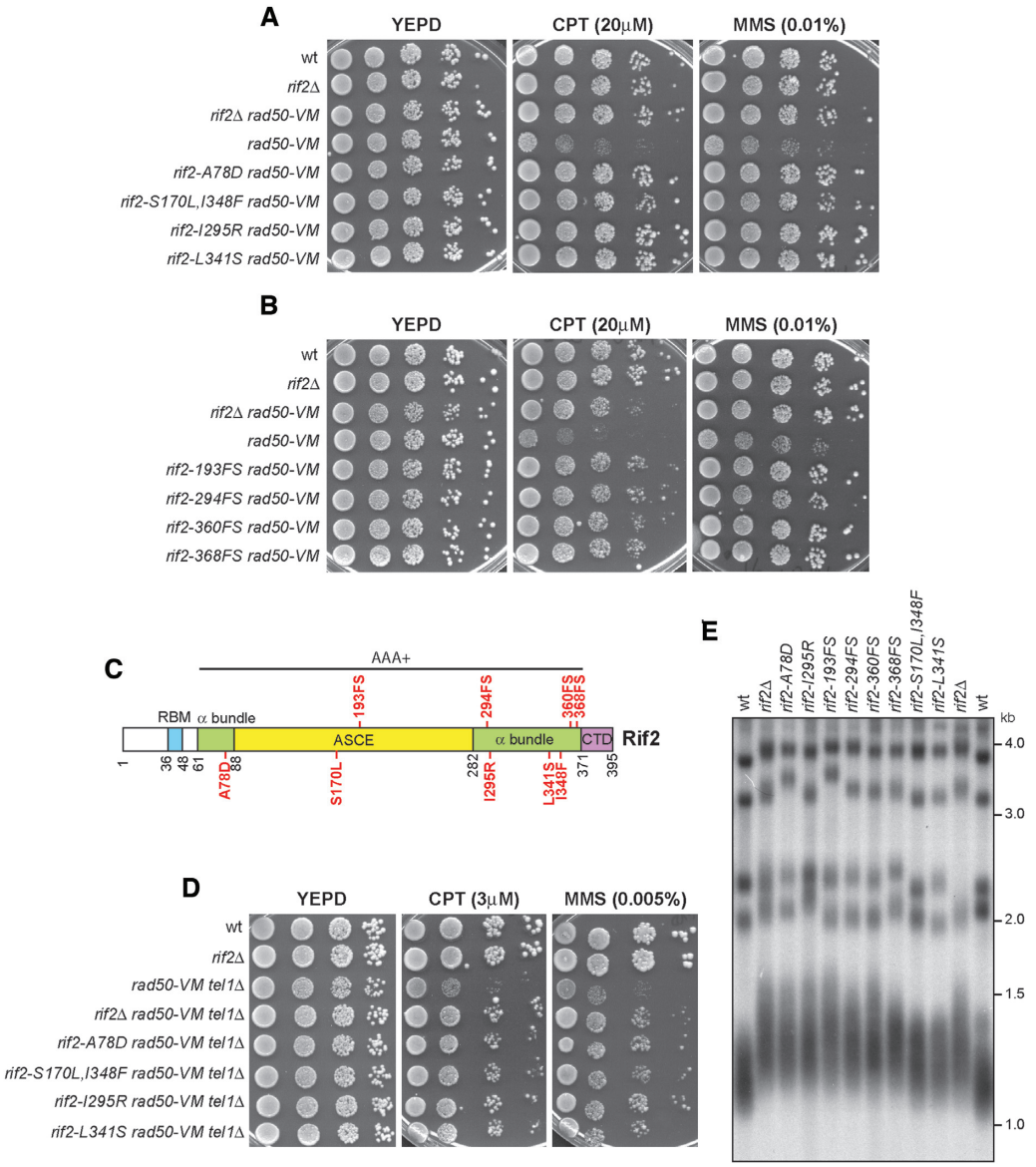

Figure 1. Identification of *rif2* alleles that suppress the DNA damage sensitivity of *rad50-VM* cells. (**A, B**) Exponentially growing cells with the indicated genotypes were serially diluted (1:10) and each dilution was spotted out onto YEPD plates with or without CPT or MMS. (**C**) Position of the mutations within the Rif2 sequence. (**D**) Exponentially growing cells were serially diluted (1:10) and each dilution was spotted out onto YEPD plates with or without CPT or MMS. (**E**) XhoI-cut genomic DNA prepared from exponentially growing cells was subjected to Southern blot analysis using a poly(GT) probe.

Rap1^{R747L}-Rif2 complex (–12.4 kcal/mol) compared to the wild type Rap1-Rif2 complex (–16.2 kcal/mol) (Figure 2C and Supplementary Figure S3A and B). Interestingly, a similar ΔG increase can be detected also in the Rap1-Rif2^{L341S} complex (–13.1 kcal/mol) (Figure 2C and Supplementary Figure S3A and C), suggesting that the Rif2 L341S mutation reduces the binding affinity between Rif2 and Rap1.

We directly tested this prediction by immunoprecipitating Rap1 from protein extracts from cells expressing either Rif2 or Rif2^{L341S} protein tagged with a Myc epitope. The amount of Rif2^{L341S} was under the detection level in Rap1 immunoprecipitates compared to wild type Rif2 (Figure 2D), indicating that the Rif2 L341S mutation impairs Rap1-Rif2 interaction.

In addition to R747L, also the H709A amino acid substitution was shown to impair Rap1-Rif2 interaction (64), whereas the D727A substitution specifically impairs the interaction between Rap1 and Rif1 (64). Consistently with the lack of Rap1-Rif2 interaction by the H709A and R747L amino acid substitutions, telomeres in *rap1-H709A* and *rap1-R747L* cells were as long as in *rif2-L341S* cells and the presence of either the *rap1-H709A* or the *rap1-R747L* allele did not further increase the length of telomeres of *rif2-L341S* cells (Figure 2E). To confirm that the lack of Rif2–Rap1 interaction is sufficient to restore DNA damage resistance of *rad50-VM* cells, we investigated the *in vivo* consequences of the *rap1-H709A*, *rap1-R747L* and *rap1-D727A* alleles. Similar to the *rif2-L341S* allele, both *rap1-H709A*

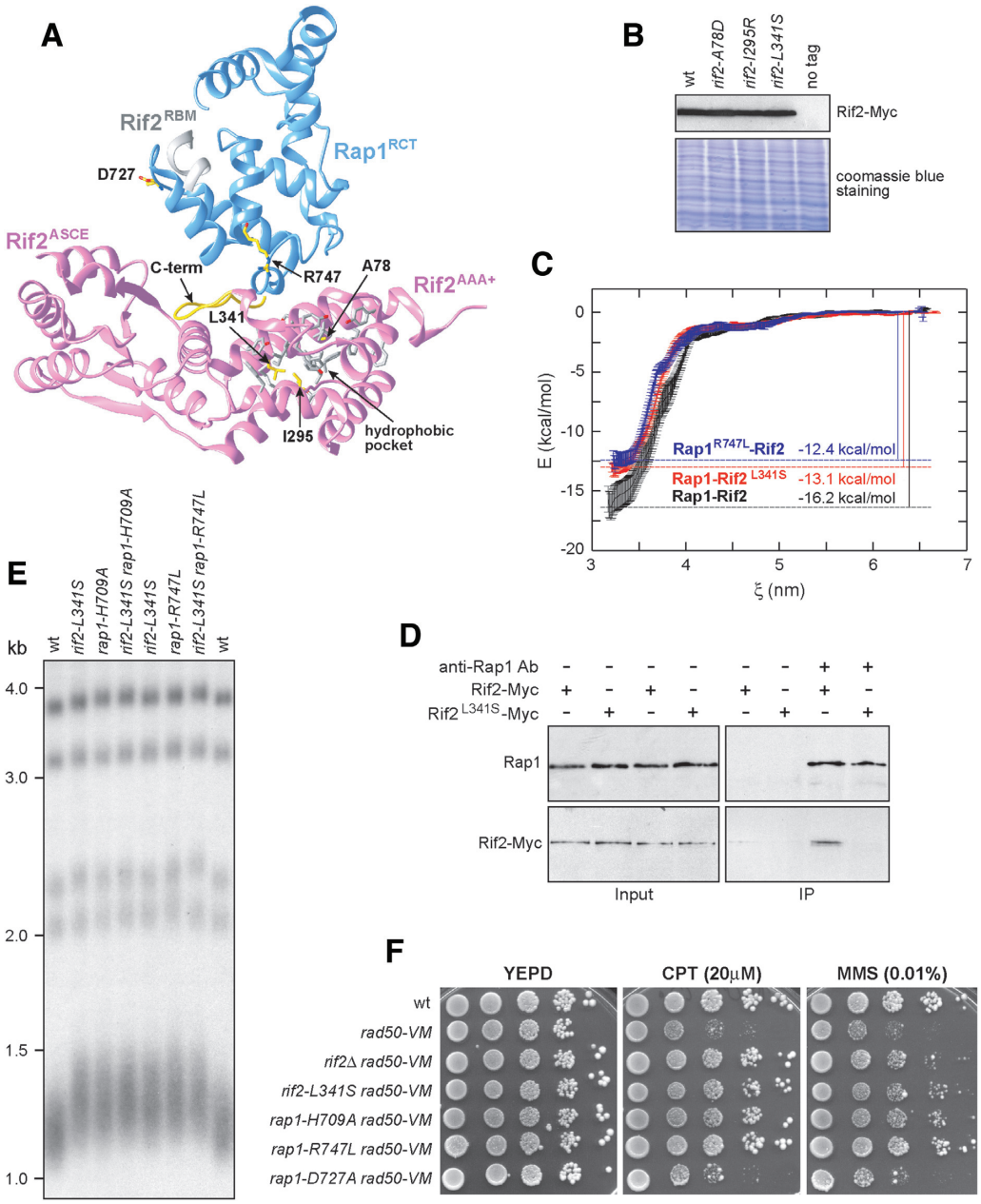

Figure 2. The lack of Rif2-Rap1 interaction restores DNA damage resistance of *rad50-VM* cells. (**A**) Structure of Rap1^{RCT} (blue) and Rif2 (pink) (PDB code: 4BJ5) complex. The residues affected by the investigated mutations are shown in yellow. (**B**) Western blot analysis with anti-Myc antibodies of protein extracts from the indicated strains. The same amount of extracts was separated on a SDS-PAGE and stained with Coomassie Blue as loading control. (**C**) Average PMF ΔG calculated using Bayesian bootstrapping of umbrella histograms for binding/unbinding of Rap1-Rif2 (in black), Rap1-Rif2^{L341S} (in red) and Rap1^{R747L}-Rif2 (in blue) complexes. Standard deviations of ΔG are indicated with vertical error bars. (**D**) Rap1-Rif2 interaction. Protein extracts prepared from exponentially growing cells expressing either Rif2-Myc or Rif2^{L341S}-Myc were analyzed by western blotting with anti-Rap1 and anti-Myc antibodies either directly (Input) or after immunoprecipitation (IP) with anti-Rap1 antibody. (**E**) XhoI-cut genomic DNA prepared from exponentially growing cells was subjected to Southern blot analysis using a poly(GT) probe. (**F**) Exponentially growing cells were serially diluted (1:10) and each dilution was spotted out onto YEPD plates with or without CPT or MMS.

and *rap1-R747L* alleles, which did not cause DNA damage hypersensitivity by themselves (Supplementary Figure S4), suppressed the CPT and MMS sensitivity of *rad50-VM* cells, whereas the *rap1-D727A* allele did not (Figure 2F). Altogether, these data indicate that the lack of Rap1-Rif2 interaction is sufficient to restore DNA damage resistance of *rad50-VM* cells.

The lack of Rif2-Rap1 interaction increases MRX association to DNA ends and restores end-tethering in *rad50-VM* cells

The *rad50-VM* mutation reduces MRX association at broken DNA ends, and *RIF2* deletion suppressed this defect (27). The finding that Rif2 L341S, Rap1 H709A and Rap1 R747L amino acid substitutions restored DNA damage

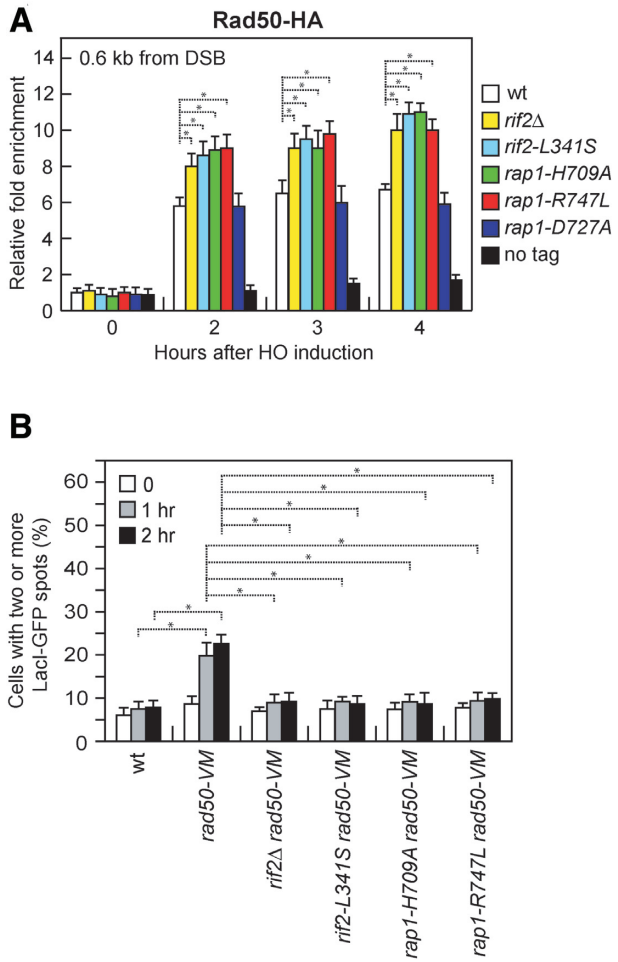

Figure 3. The lack of Rif2-Rap1 interaction increases MRX association to DSBs and restores end-tethering in *rad50-VM* cells. (**A**) ChIP analysis. Exponentially growing YEPR cells were transferred to YEPRG at time zero to induce HO. Relative fold enrichment of Rad50-HA fusion protein at the indicated distances from the HO cleavage site was determined after ChIP with anti-HA antibody and qPCR. (**B**) End-tethering. Exponentially growing YEPR cell cultures were arrested in G2 with nocodazole at time zero and transferred to YEPRG in the presence of nocodazole. Two hundred cells for each strain were analyzed to determine the percentage of cells showing two or more LacI-GFP foci. In all graphs, mean values are represented with error bars denoting s.d. ($n = 3$). *$P < 0.05$ (Student's *t*-test).

resistance of *rad50-VM* cells prompted us to investigate whether they also increased MRX persistence at DSBs. To detect MRX association at the DSB ends, we used JKM139 derivative strains, where a single DSB at the *MAT* locus can be generated by expression of the *HO* endonuclease gene under the control of a galactose-inducible promoter (65). To avoid the influence of DSB repair, this HO-induced DSB cannot be repaired by HR because the homologous donor loci *HML* and *HMR* are deleted. Furthermore, galactose was maintained in the medium to re-cleave the HO sites that were eventually reconstituted by NHEJ. Chromatin immunoprecipitation (ChIP) and quantitative real time PCR (qPCR) showed that, similar to *rif2Δ* cells, *rif2-L341S*, *rap1-H709A* and *rap1-R747L* cells increased Rad50 association at the HO-induced DSB compared to wild type cells (Figure 3A). By contrast, Rad50 association to DSBs was not enhanced by the *rap1-D727A* allele (Figure 3A), which did not restore DNA damage resistance of *rad50-VM* cells (Figure 2F). Thus, Rif2 appears to need to interact with Rap1 in order to negatively regulate MRX association to DSBs.

The poor MRX association at DSBs in *rad50-VM* cells does not impair DSB resection (27), while *rad50-VM* cells are defective in keeping the DSB ends tethered to each other (27). Thus, we asked whether the Rif2^{L341S}, Rap1^{H709A} and Rap1^{R747L} variants could restore DNA damage resistance of *rad50-VM* cells by suppressing their end-tethering defect. To this end, we used a yeast strain harboring a galactose-inducible HO endonuclease and an HO cleavage site at chromosome VII (66). This strain was deleted for the endogenous HO sites at the *MAT*, *HML* and *HMR* loci on chromosome III to ensure that the broken chromosomal fragments did not recombine with these loci. The DNA proximal to the HO-induced DSB can be visualized by binding of LacI-GFP fusion protein to multiple repeats of the LacI repressor binding site, *LacO*, that are integrated on both sides of the HO break site (66). HO was induced by galactose addition to cells that were arrested in G2 with nocodazole and kept blocked in G2 by nocodazole treatment in order to ensure that all cells would arrest in metaphase. The majority of wild-type cells showed a single LacI-GFP focus both before and after HO induction, indicating their ability to keep the broken DNA ends together (Figure 3B). Consistently with previous results (27), *rad50-VM* cells showed an increase of two LacI-GFP spots at 1–2 h after HO induction (Figure 3B), indicating an end-tethering defect. Similar to *rif2Δ*, the presence of the *rif2-L341S*, *rap1-H709A* or *rap1-R747L* allele reduced the number of *rad50-VM* cells showing two LacI-GFP spots after HO induction (Figure 3B), indicating that these *rif2* and *rap1* alleles suppressed the *rad50-VM* end-tethering defect. As the maintenance of the DSB ends in close proximity is important to repair a DSB by both NHEJ and HR (66–69), this restored end-tethering could explain the suppression of the DNA damage sensitivity of *rad50-VM* cells by the corresponding Rif2^{L341S}, Rap1^{H709A} and Rap1^{R747L} variants.

Rap1 binds to DSBs and promotes Rif2 association to them

Rif2 was shown to associate to DSBs, spreading to 2 kb from the HO cleavage site (27). Because the lack of Rap1-Rif2 interaction is sufficient to increase both DNA damage resistance of *rad50-VM* cells and MRX association to DSBs, we asked whether Rap1 is bound at DSBs and promotes Rif2 association to them. In fact, although Rap1 is known to bind a DNA recognition sequence consisting of two half-sites of 5 bp separated by 1 or 3 bp, it is also capable to bind *in vitro* a single half-site (48) or even a random ds-DNA sequence (49). Following HO induction by galactose addition, Rap1 was efficiently recruited close to the HO-induced DSB (Figure 4A). Furthermore, the Rap1^{H709A} and Rap1^{R747L} variants reduced Rif2 association at both the HO-induced DSB (Figure 4B) and telomeres (Figure 4C), whereas Rap1^{D727A} did not (Figure 4B and C). This reduced Rif2 association at both DSBs and telomeres is not due to different amount of Rap1 or Rif2 protein, as similar amounts of Rap1 and Rif2 proteins could be detected in

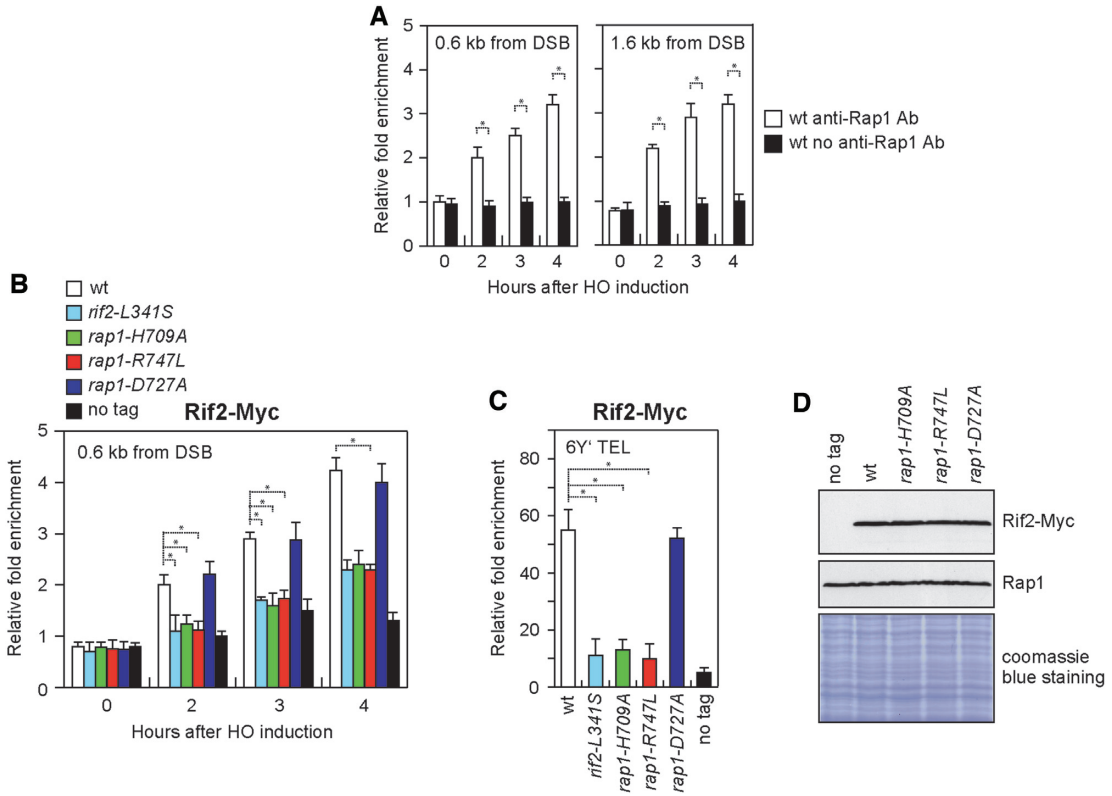

Figure 4. Rap1 is recruited to DSB ends and mediates Rif2 association at both DSBs and telomeres. (**A**) Exponentially growing YEPR cell cultures were transferred to YEPRG at time zero to induce HO. Relative fold enrichment of Rap1 at the indicated distances from the HO cleavage site was determined after ChIP with anti-Rap1 antibody and qPCR. (**B**) As in A, but showing Rif2-Myc. (**C**) Relative fold enrichment of Rif2-Myc at six different Y'-containing telomeres (6Y') compared to a non-telomeric locus (*ARO1*) after ChIP with anti-Myc antibody and qPCR. (**D**) Western blot analysis with anti-Myc and anti-Rap1 antibodies of extracts used for the ChIP analysis shown in (B and C). The same amounts of extracts were separated on a SDS-PAGE and stained with Coomassie Blue as loading control. In all graphs, mean values are represented with error bars denoting s.d. ($n = 3$). *$P < 0.05$ (Student's *t*-test).

protein extracts from wild type, *rap1-H709A*, *rap1-R747L* and *rap1-D727A* cells (Figure 4D). Finally, the Rif2 L341S amino acid substitution, which impaired Rif2-Rap1 interaction (Figure 2C and D), decreased Rif2 association at both the HO-induced DSB (Figure 4B) and telomeres (Figure 4C). Thus, Rap1 supports Rif2 functions in controlling MRX activity by promoting Rif2 association/persistence at DSBs.

The Rap1 R381W, P520L and D555N mutations exacerbate the DNA damage sensitivity and the end-tethering defect of *rad50-VM* cells by reducing MRX association to DSBs

As Rap1 is essential for cell viability, to better understand the function of Rap1 at DSBs, we searched for *rap1* mutations that either suppressed or exacerbated the hypersensitivity to DNA damaging agents of *rad50-VM* cells. We used low-fidelity PCR to randomly mutagenize *RAP1* gene and *rad50-VM* cells were transformed with the *RAP1* PCR products in order to substitute the corresponding *RAP1* wild type sequence with the mutagenized DNA fragments. Transformants clones were then screened for either increased or decreased viability in the presence of CPT compared to *rad50-VM* cells. This screen yielded three *rap1* alleles exacerbating the sensitivity of *rad50-VM* cells not only to CPT but also to MMS (Figure 5A), whereas no *rap1* alleles restoring DNA damage resistance in the same cells were identified. All the identified *rap1* alleles also exacerbated the CPT and MMS hypersensitivity of *rad50-VM tel1Δ* (Figure 5B), indicating that this effect does not require Tel1. Sequence analysis revealed that the three *rap1* alleles contained single missense mutations resulting in the amino acid changes R381W, P520L or D555N, which are all located in the Rap1 DNA binding domain (Figure 5C).

As the R381W, P520L and D555N amino acid substitutions sensitized *rad50-VM* cells to DNA damaging agents, we investigated whether they decreased MRX association to DSBs. This was indeed the case. In fact, although similar amounts of Rad50 could be detected in protein extracts from wild type, *rap1-R381W*, *rap1-P520L* and *rap1-D555N* cells (Figure 5D), the amount of Rad50 bound at the HO-induced DSB was decreased in *rap1-R381W*, *rap1-P520L* and *rap1-D555N* cells compared to wild type cells (Figure 5E).

As both $Rap1^{R381W}$ and $Rap1^{P520L}$ exacerbated the DNA damage sensitivity of *rad50-VM* cells (Figure 5A) and decreased MRX association to DSBs (Figure 5E), we asked whether they impair end-tethering and/or exacerbate the end-tethering defect of *rad50-VM* cells. As expected, *rad50-VM* cells showed an increase of two LacI-GFP spots after HO induction compared to wild-type cells (Figure 5F). A similar increase in the frequency of two LacI-GFP foci

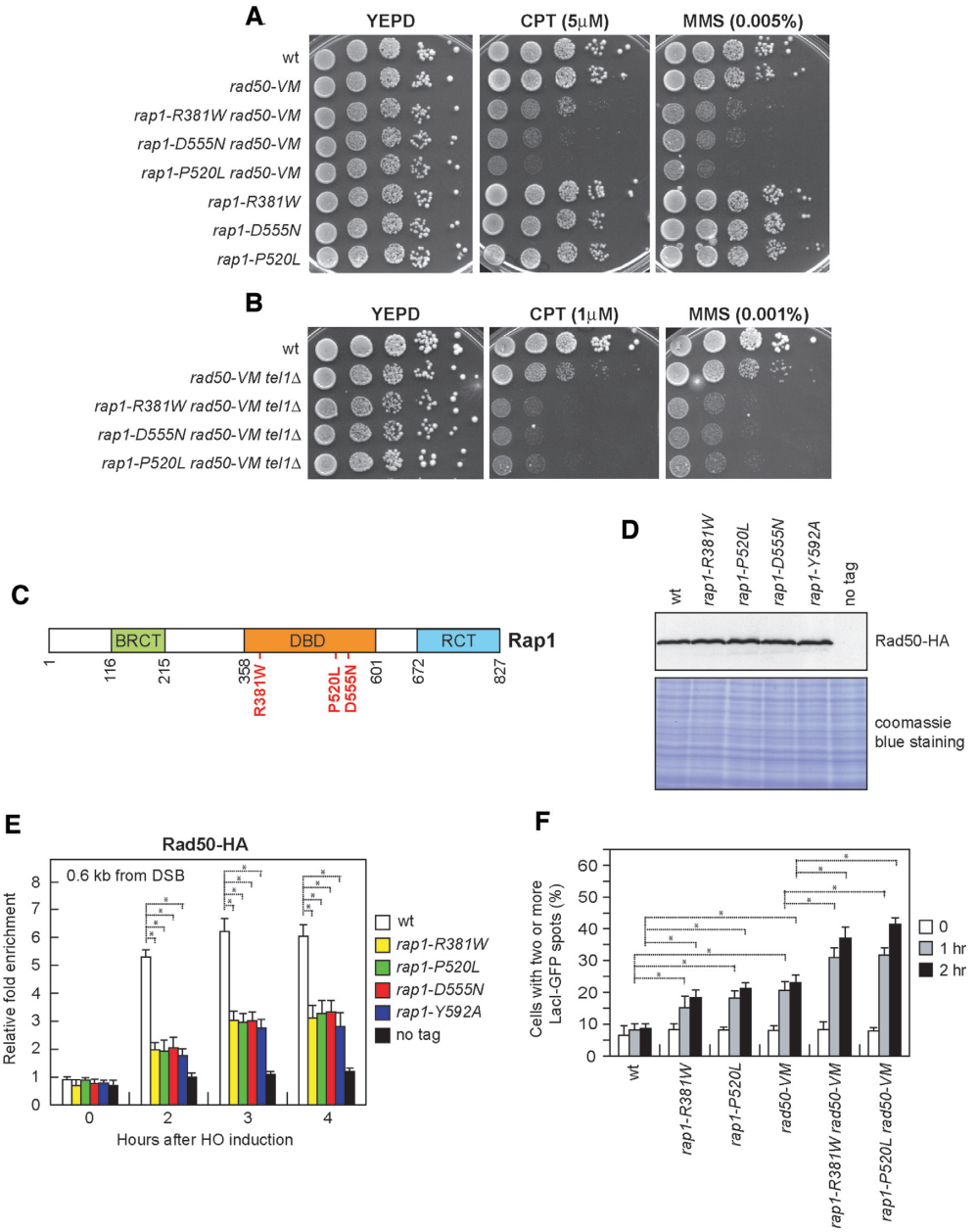

Figure 5. Identification of *rap1* alleles that exacerbate the DNA damage sensitivity of *rad50-VM* cells by decreasing MRX association to DSBs. (**A, B**) Exponentially growing cells were serially diluted (1:10) and each dilution was spotted out onto YEPD plates with or without CPT or MMS. (**C**) Position of the mutations within the Rap1 sequence. (**D**) Western blot analysis with anti-HA antibodies of extracts used for the ChIP analysis shown in (E). The same amounts of extracts were separated on a SDS-PAGE and stained with Coomassie Blue as loading control. (**E**) ChIP analysis. Exponentially growing YEPR cell cultures were transferred to YEPRG at time zero to induce HO. Relative fold enrichment of Rad50-HA at the indicated distance from the HO cleavage site was determined after ChIP with anti-HA antibody and qPCR. (**F**) End-tethering. Exponentially growing YEPR cell cultures were arrested in G2 with nocodazole at time zero and transferred to YEPRG in the presence of nocodazole. 200 cells for each strain were analyzed to determine the percentage of cells showing two or more LacI-GFP foci. In all graphs, mean values are represented with error bars denoting s.d. ($n = 3$). *$P < 0.05$ (Student's *t*-test).

was observed also in *rap1-R381W* and *rap1-P520L* cells compared to wild type (Figure 5F), indicating an end-tethering defect. This frequency was further increased in *rap1-R381W rad50-VM* and *rap1-P520L rad50-VM* double mutants compared to each single mutant (Figure 5F), suggesting that the increased DNA damage sensitivity of the double mutants compared to each single mutant can be due to a more severe end-tethering defect.

The Rap1 R381W and P520L mutations cause hypersilencing and telomere shortening

The finding that *rap1-R381W*, *rap1-P520L* and *rap1-D555N* mutant cells display phenotypes opposite to *rif2* or *rap1* alleles impairing Rap1 or Rif2 interaction, respectively, suggests that they may encode hypermorphic Rap1 mutant variants. As Rap1 dysfunction can lead to telomere lengthening (33,35) and loss of silencing at both *HM*

loci and telomeres (32–34), we tested the above hypothesis by evaluating these two processes in the mutants. While, as expected (28,34), the lack of Rap1^{RCT} (*rap1-ΔC* in Figure 6A), which mediates Rap1 interaction with Rif1 and Rif2, caused telomere overelongation, telomeres in *rap1-R381W* and *rap1-P520L* cells were shorter than in wild type cells, whereas the *rap1-D555N* allele did not alter telomere length (Figure 6A).

To examine transcriptional silencing, we inserted the *rap1* alleles in strains carrying the only copy of the *URA3* gene inserted next to the left telomere of chromosome VII or at the *HMLα* locus (70). Repression of *URA3* expression can be detected by testing the ability of cells to form colonies on 5-fluoroorotic acid (5-FOA), which kills *URA3* expressing cells. The *rap1-R381W*, *rap1-P520L* and *rap1-D555N* mutants showed increased *URA3* silencing at both *HMLα* (Figure 6B) and telomeres (Figure 6C) compared to wild type. Hypersilencing in all the above *rap1* mutants was completely dependent on Sir proteins, as the lack of *SIR3* abolished the ability of *rap1-R381W*, *rap1-P520L* and *rap1-D555N* cells to form colonies on 5-FOA (Figure 6C). Altogether, these findings indicate that the *rap1-R381W*, *rap1-P520L* and *rap1-D555N* alleles encode hypermorphic Rap1 variants that increase Rap1 functions in both telomerase repression and transcriptional silencing at *HM* loci and at telomeres.

Next, we measured the association of Rap1^{R381W}, Rap1^{P520L} and Rap1^{D555N} to both DSBs and telomeres by ChIP analysis and qPCR. Although the R381W, P520L and D555N mutations did not alter Rap1 protein level (Figure 6D), the amount of Rap1^{R381W}, Rap1^{P520L} and Rap1^{D555N} bound at the HO-induced DSB was higher than that of wild type Rap1 (Figure 6E). Similarly, the R381W, P520L and D555N mutations increased Rap1 association at telomeres (Figure 6F). These findings suggest that the increased ability of these Rap1 variants to inhibit telomere elongation and MRX association at both telomeres and DSBs, as well as to repress transcription at least at telomeres could be due to their enhanced persistence to DNA ends.

The Rap1 R381W and P520L mutations change the affinity of Myb-like domains for DNA in opposite manners

The Rap1^{DBD} consists of two tandem Myb-like motifs, followed by a C-terminal wrapping loop (45–47). While R381 resides in the N-terminal Myb-like domain (Myb-N), P520 and D555 are localized in the C-terminal Myb-like domain (Myb-C) (PDB code: 3UKG) (Figure 7A). In particular, R381 forms several hydrogen bonds with surrounding residues, likely conferring stability to the helix-loop-helix folding. By contrast, P520 is localized in a quite rigid loop surrounding the C-terminal Myb-like domain, facing the DNA but with no significant interaction with it. Finally, the D555 residue is situated on the other side of the Myb-C domain, on the side not facing the DNA (Figure 7A), and its role is not trivial to speculate.

We focused on R381W and P520L mutations to test their effect on the DNA binding properties of Myb-N and Myb-C domains by biased molecular dynamics simulations. Models representing Myb-N or Myb-C domain bound to DNA were generated starting from the structure of Rap1^{DBD} bound to telomeric DNA (PDB code 3UKG). The R381W mutation was introduced in the Myb-N model, whereas the P520L mutation was introduced in the Myb-C model. PMF was calculated both for DNA-Myb-N^{R381W} (Figure 7B and Supplementary Figure S5) and DNA-Myb-C^{P520L} (Figure 7C and Supplementary Figure S6) and these PMFs were compared with those of wild type DNA-Myb-N and wild type DNA-Myb-C, respectively. Consistently with the ChIP results showing increased Rap1^{R381W} binding at both DSBs and telomeres compared to wild type Rap1 (Figure 6E and F), the R381W mutation increases the binding affinity of Myb-N for dsDNA, reducing the ΔG from −17.1 kcal/mol to −23.3 kcal/mol (Figure 7B). By contrast, although Rap1^{P520L} showed increased association at both DSBs and telomeres by ChIP (Figure 6E and F), the P520L mutation appears to significantly decrease the stability of the DNA–Myb-C complex by increasing the ΔG from −20.0 kcal/mol to −13.4 kcal/mol (Figure 7C), suggesting that this mutation decreases the binding affinity of the Myb-C domain for dsDNA.

The Rap1 P520L mutation favours formation of high Rap1 stoichiometry complexes on DNA

The Rap1^{DBD} domain binds dsDNA molecules *in vitro* in two different binding modes: a high affinity mode, where the two Myb-like domains both bind dsDNA, and a low affinity mode, where only a single Myb-like domain binds dsDNA (49,50). The presence of a single Myb-like domain on dsDNA has been proposed to allow the binding of multiple Rap1 molecules leading to the formation of Rap1-DNA complexes with high stoichiometry (49,50). As the P520L mutation appears to decrease the affinity of Myb-C for DNA, the increased Rap1^{P520L} association to both DSBs and telomeres detected by ChIP might be due to a destabilization of the clamped structure of Rap1^{DBD}, which would facilitate the binding of multiple Rap1 molecules in a conformation where only Myb-N takes contact to DNA. We therefore analyzed the consequence of P520L amino acid substitution on Rap1^{DBD} ability to bind dsDNA by gel electrophoretic mobility shift assay (EMSA). Both wild type and mutant Rap1^{DBD} domains, comprising residues 358–601, were expressed and purified from *Escherichia coli* cells as soluble proteins (Supplementary Figure S7) and tested for the ability to bind a 21 bp dsDNA substrate carrying the canonical telomeric Rap1 DNA recognition sequence consisting of two hemisites spaced by 3 bp. A fixed amount of DNA binding site was incubated with increasing concentrations of purified Rap1^{DBD} and complex formation was analyzed by EMSA. As previously reported (46,49,50), wild type Rap1^{DBD} was capable to form a 1:1 DBD–DNA complex and increasing Rap1 concentration revealed the appearance of a second faint band (2:1), possibly representing the binding to DNA of more than one DBD molecule (Figure 7D). By contrast, DBD^{P520L} showed a reduction of 1:1 DBD–DNA complex and the appearance not only of a second (2:1) but also of a third (3:1) band (Figure 7D), suggesting that the P520L amino acid substitution favours transition to higher order DBD^{P520L}–DNA complexes.

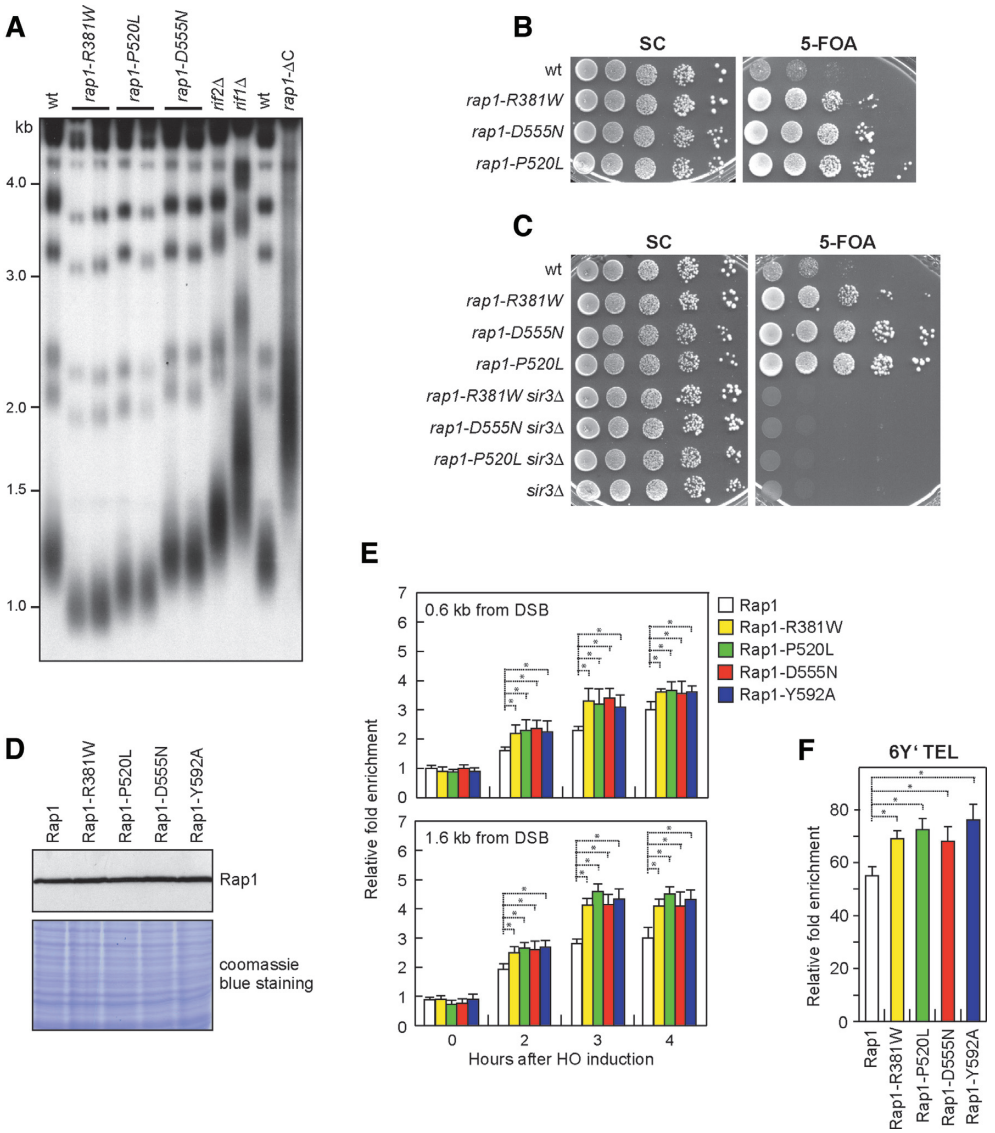

Figure 6. Effects of the *rap1* alleles on telomere length and transcriptional silencing. (**A**) XhoI-cut genomic DNA prepared from exponentially growing cells was subjected to Southern blot analysis using a poly(GT) probe. (**B, C**) Exponentially growing cells carrying the *URA3* gene at the *HML*α locus (B) or at telomere VII-L (C) were serially diluted (1:10) and each dilution was spotted out onto complete synthetic medium (SC) and onto the same medium supplied with 5-FOA (5-FOA) to assay for *URA3* expression. (**D**) Western blot analysis with anti-Rap1 antibodies of extracts used for the ChIP analysis shown in (E and F). (**E**) ChIP analysis. Exponentially growing YEPR cell cultures were transferred to YEPRG at time zero to induce HO. Relative fold enrichment of the indicated proteins at the indicated distances from the HO cleavage site was determined after ChIP with anti-Rap1 antibody and qPCR. (**F**) Relative fold enrichment of the indicated protein at six different Y'-containing telomeres (6Y') compared to a non-telomeric locus (*ARO1*) after ChIP with anti-Rap1 antibody and qPCR analysis. In all graphs, plotted values are the mean values with error bars denoting s.d. ($n = 3$). *$P < 0.05$ (Student's *t*-test).

Destabilization of the wrapping loop increases Rap1 association to DNA ends and Rap1 activation

As removal of the wrapping loop was shown to favour the transition to a high stoichiometry binding mode (50), we investigated the consequences of substituting to alanine the Rap1 Y592 residue, which is located on the tip of the loop and contributes to lock the loop around DNA (Figure 7A) (47). The Y592A mutation turned out to increase the DNA damage sensitivity of *rad50-VM* cells (Figure 8A) and to reduce Rad50 association to DSBs (Figure 5E) without altering Rad50 protein level (Figure 5D). Furthermore, although this mutation was shown to decrease Rap1 affinity for dsDNA *in vitro* (47), the amount of Rap1^{Y592A} bound at both DSBs and telomeres, as measured by ChIP and qPCR, was higher than that of wild type Rap1 (Figure 6E and F). This effect was not due to increased level of the mutant protein, as similar amounts of Rap1 were detected in protein extracts from wild type and *rap1-Y592A* cells (Figure 6D).

As *rap1-Y592A* cells showed reduced cell viability even in the absence of DNA damaging agents (Figure 8A), we could not test their ability to grow on 5-FOA, but we assessed the effect of the Y592A mutation on silencing by evaluating the expression of the *ADE2* reporter gene integrated into a telomeric region using a color-based system (70). Expres-

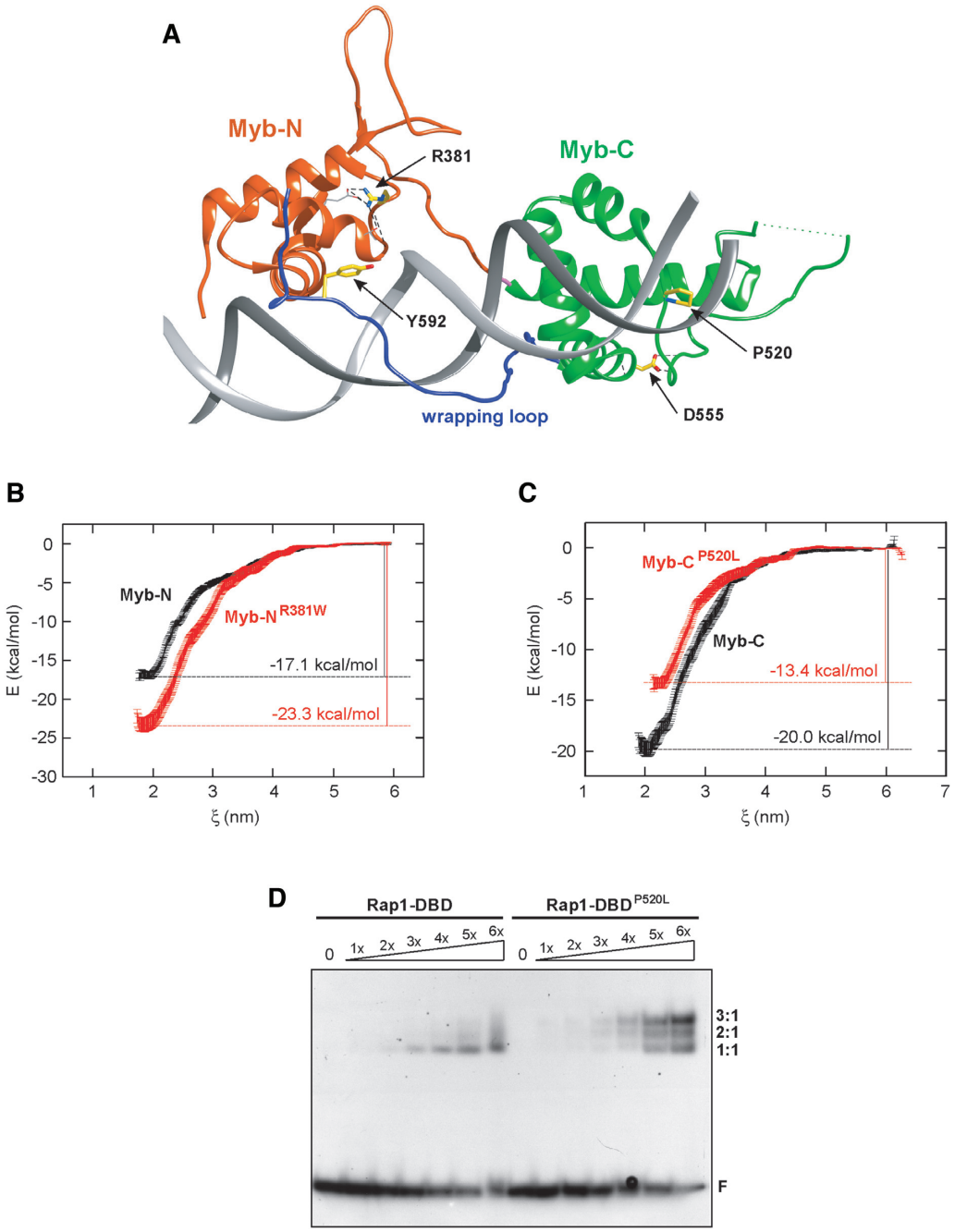

Figure 7. Effect of the Rap1 R381W and P520L mutations on the DNA binding properties of the Myb-like domains. (**A**) Structure of the high affinity complex between Rap1^{DBD} and telomeric DNA (PDB code: 3UKG). The residues affected by the investigated mutations are shown in yellow. (**B**) Average PMF ΔG calculated using Bayesian bootstrapping of umbrella histograms for binding/unbinding of DNA-Myb-N (black) and DNA-Myb-N^{R381W} (red) complexes. (**C**) Average PMF ΔG calculated using Bayesian bootstrapping of umbrella histograms for binding/unbinding of DNA-Myb-C (black) and DNA-Myb-C^{P520L} (red) complexes. In B and C, standard deviations of ΔG are indicated with vertical error bars. (**D**) EMSA with a 21 bp dsDNA and increasing concentrations of Rap1-DBD and Rap1-DBD^{P520L}. Bands corresponding to free DNA (F), and protein–DNA complexes with different stoichiometry (1:1; 2:1; 3:1) are denoted.

sion of *ADE2* results in white colonies, whereas cells that do not express *ADE2* form red-pigmented colonies. When the *ADE2* gene was placed on a telomere such that *ADE2* transcription was directed toward the telomere, cells developed sectored colonies due to transcriptional silencing (70). The *rap1-Y592A* allele was introduced in UCC3537 strain, carrying the only copy of the *ADE2* gene inserted into the telomeric region of chromosome V-R. As shown in Figure 8B, most of wild type colonies were white or red-sectored indicating that the *ADE2* gene was expressed in most cells. By contrast, most *rap1-Y592A* mutant colonies were completely red, indicating that the telomere-associated *ADE2* gene was transcriptionally silent. The hypersilencing phenotype displayed by *rap1-Y592A* cells was dependent on Sir

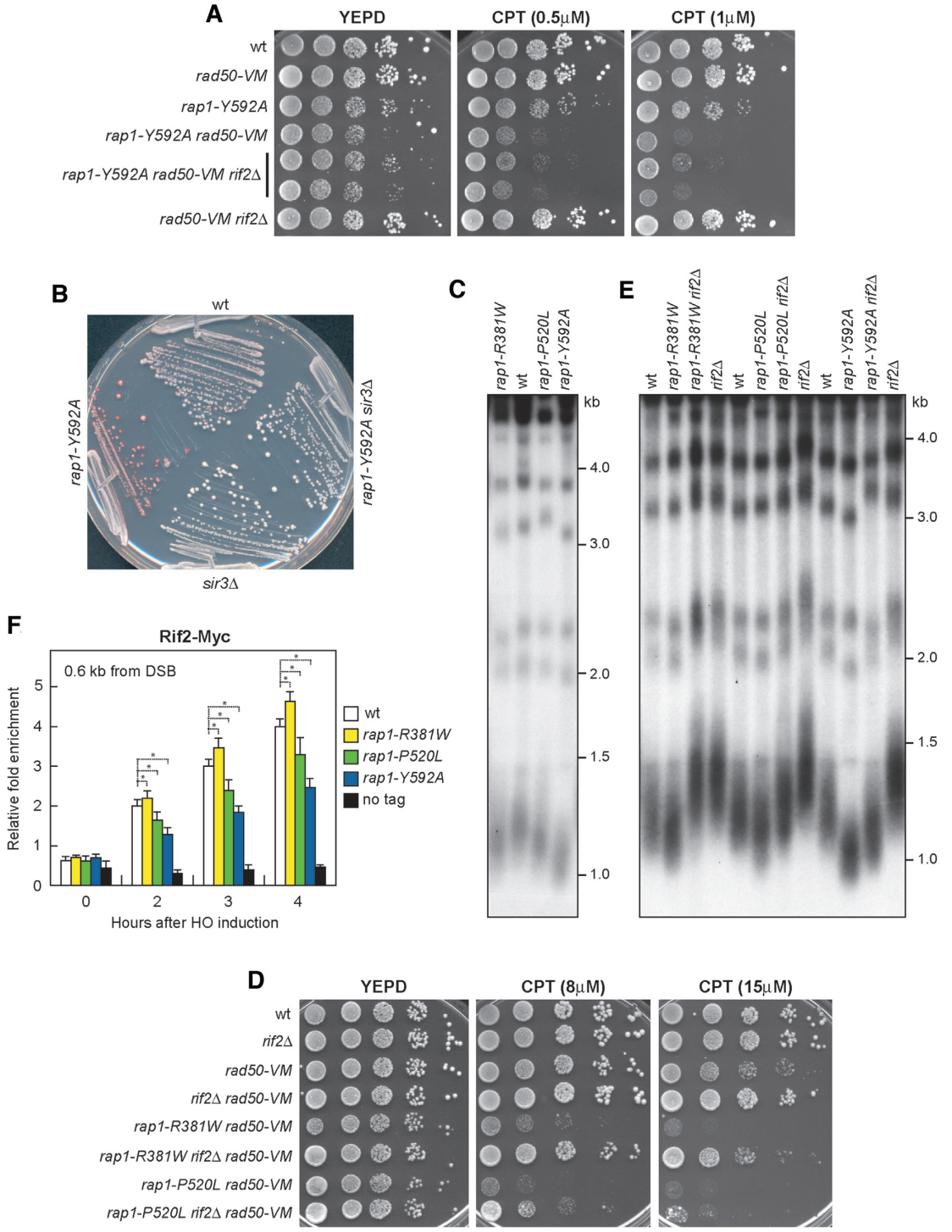

Figure 8. Effect of the *rap1-Y592A* mutation on *rad50-VM* DNA damage sensitivity, transcriptional silencing, telomere length and Rif2 association to DSBs. (**A**) Exponentially growing cells were serially diluted (1:10) and each dilution was spotted out onto YEPD plates with or without CPT. (**B**) Cells carrying the *ADE2* gene at telomere V-R were streaked onto SC plates containing a limiting amount of adenine. (**C**) XhoI-cut genomic DNA prepared from exponentially growing cells was subjected to Southern blot analysis using a poly(GT) probe. (**D**) Exponentially growing cells were serially diluted (1:10) and each dilution was spotted out onto YEPD plates with or without CPT. (**E**) XhoI-cut genomic DNA prepared from exponentially growing cells was subjected to Southern blot analysis using a poly(GT) probe. (**F**) ChIP analysis. Exponentially growing YEPR cell cultures were transferred to YEPRG at time zero. Relative fold enrichment of Rif2 at the indicated distances from the HO cleavage site was determined after ChIP with anti-Myc antibody and subsequent qPCR analysis. The mean values are represented with error bars denoting s.d. ($n = 3$). *$P < 0.05$ (Student's *t*-test).

proteins, as *rap1-Y592A* cells were unable to generate red or sectored colonies in the absence of *SIR3* (Figure 8B).

The Y592A mutation also lead to telomere shortening, as telomeres in *rap1-Y592A* cells were shorter than in wild type and even shorter than in *rap1-R381W* and *rap1-P520L* cells (Figure 8C). Altogether, these data indicate that destabilization of the wrapping domain results in phenotypes similar to those found in the presence of the Rap1^{P520L} variant.

Rap1^{P520L} and Rap1^{Y592A}, but not Rap1^{R381W}, act at both DSBs and telomeres independently of Rif2

Structural studies have shown that the interaction of both Rap1 Myb-like domains with DNA leads to an orientation of the RCT domain almost perpendicular to the DNA axis and this configuration has been proposed to favour RCT interaction with its partners (47). As Rap1 binds Rif2 through the RCT domain, the above hypothesis raises the possibility that both Rap1^{P520L} and Rap1^{Y592A}, which should bind DNA *via* a single Myb-like domain, may be defective in recruiting Rif2 to DNA, whereas Rap1^{R381W}, which should bind DNA with both Myb-like domains, should be able to do it.

We thus investigated whether Rap1^{R381W}, Rap1^{P520L} and/or Rap1^{Y592A} proteins required Rif2 to sensitize *rad50-VM* cells to DNA damaging agents and/or to cause telomere shortening. As expected, *rap1-R381W rad50-VM* cells were more sensitive to DNA damaging agents compared to *rad50-VM* cells (Figure 8D). *RIF2* deletion restored DNA damage resistance not only in *rad50-VM* but also in *rap1-R381W rad50-VM* cells (Figure 8D), indicating that Rap1-R381W needs Rif2 to sensitize *rad50-VM* cells to DNA damaging agents. Furthermore, while *rap1-R381W* cells displayed short telomeres, telomeres in *rif2Δ rap1-R381W* cells were as long as in *rif2Δ* cells (Figure 8E). Thus, Rap1^{R381W} appears to act through Rif2 to negatively regulate both MRX function at DSBs and telomere length.

By contrast, *RIF2* deletion was almost unable to restore DNA damage resistance of *rad50-VM* cells carrying the *rap1-Y592A* (Figure 8A) or *rap1-P520L* allele (Figure 8D), indicating that Rap1^{P520L} and Rap1^{Y592A} sensitize *rad50-VM* cells in a Rif2-independent manner. Furthermore, telomeres in *rif2Δ rap1-P520L* and *rif2Δ rap1-Y592A* cells were shorter than in *rif2Δ* cells, although not as short as in *rap1-P520L* and *rap1-Y592A* cells, respectively, indicating that Rap1^{P520L} and Rap1^{Y592A} are capable of inhibiting telomerase even in the absence of Rif2 (Figure 8E).

Consistent with the finding that Rap1^{R381W} acts in a Rif2-dependent manner, the amount of Rif2 bound at DSBs was increased in *rap1-R381W* cells (Figure 8F) and this is in agreement with the increased Rap1^{R381W} association to DSBs (Figure 6E). By contrast, both *rap1-P520L* and *rap1-Y592A* cells showed reduced Rif2 accumulation at DSBs (Figure 8F), with *rap1-Y592A* cells showing the major effect, suggesting that the release of the RCT domain from the DBD closure influences the ability of Rap1 to load Rif2 on dsDNA.

DISCUSSION

In both yeast and mammals, the MRX complex and Tel1 are rapidly recruited to DSBs to initiate repair events and checkpoint signaling (6). Both MRX and Tel1 are also involved in telomere maintenance by allowing access of telomerase to the telomere (17). We and others have shown that MRX association at both DSBs and telomeres is negatively regulated by Rif2 (25,27), which is recruited to telomeres by the DNA binding protein Rap1 (28).

Rap1 dysfunction has been shown to cause MRX-mediated telomere degradation (51,52), suggesting that Rap1 can be involved in repressing MRX activity at least at telomeres. Whether Rap1 also acts at DSBs is unknown. Here we show that Rif2 needs Rap1 to repress MRX association at both DSBs and telomeres. In fact, *rif2* or *rap1* alleles specifically impaired in Rap1 or Rif2 interaction, respectively, behave like *RIF2* deletion in increasing MRX association at DSBs. This enhanced MRX persistence suppresses the DNA damage hypersensitivity and the end-tethering defect caused by the *rad50-VM* mutation, which is known to reduce MRX association to DSBs. Importantly, Rap1 is recruited to DNA DSBs and promotes Rif2 association to them, thus explaining the reason why Rap1 is required to support Rif2 activity at DSBs. The lack of this Rap1/Rif2-mediated inhibition of MRX retention at DSBs not only suppresses the end-tethering defect of *rad50-VM* cells, but it also increases the efficiency of end-tethering and NHEJ in wild type cells (27). This finding suggests that inhibition of MRX association at DSBs by Rap1 and Rif2 can be important in the regulation of the choice between DSB repair by HR and NHEJ.

Rif2 has been proposed to inhibit MRX association/persistence to DNA ends by two different mechanisms: (i) it counteracts Tel1-mediated stabilization of MRX association to DSBs, possibly by competing with Tel1 for MRX binding (25–27); (ii) it discharges the ATP-bound form of MRX, which is important to support the DNA binding activity of the complex, by enhancing ATPase activity by Rad50 in a Tel1-independent manner (27,29). The finding that *rif2* and *rap1* alleles specifically impaired in Rap1 or Rif2 interaction, respectively, do not need Tel1 to restore DNA damage resistance of *rad50-VM* cells suggests that their suppression effect could be due at least in part to their failure to enhance ATPase activity by Rad50.

Crystal structures have shown that Rap1 binds telomeric DNA in a high-affinity mode through both tandem Myb-like domains, with the wrapping loop locking Rap1 around DNA by interacting with Myb-N (45–47). However, the transient opening of the wrapping loop allows Rap1 to bind *in vitro* both telomeric and non-telomeric DNA sequences through only one Myb-like domain leading to formation of Rap1-DNA complexes with high stoichiometry (48–50). Whether this alternative binding mode can be adopted *in vivo* and/or it plays any functional role is hitherto unknown.

We provide evidence that Rap1 functions at DNA ends are influenced by its DNA binding mode. In fact, ChIP analyses have shown that the Rap1 R381W and P520L mutations, which cause enhanced Rap1 activity in counteracting telomere elongation and in repressing both MRX association at DNA ends and gene expression, increase the amount of Rap1 bound to DNA ends. However, biased molecular dynamics simulations indicate that, while the R381W mutation enhances Myb-N affinity for DNA,

thus straightforwardly explaining the increased Rap1^{R381W} association to DSBs observed by ChIP, the P520L mutation decreases Myb-C affinity for DNA. Importantly, gel electrophoretic mobility shift assays show that Rap1 DBD^{P520L} favours formation of Rap1^{DBD}-DNA complexes with higher stoichiometry. These findings suggest that the increased amount of chromatin bound Rap1^{P520L} detected by ChIP is due to destabilization of the Rap1 clamped structure that results in an easier transition to Rap1-DNA complexes with high stoichiometry, where only Myb-N makes contacts with DNA. Consistently with this hypothesis, opening of the wrapping loop through the Y592A mutation leads to similar phenotypes, i.e. increased Rap1 association to DSBs, decreased MRX association to DSBs, telomere shortening and hypersilencing. Altogether, these findings indicate that, depending of its DNA binding mode, Rap1 can form protein–DNA complexes with different functional properties. As Rap1 is capable to bind also random dsDNA sequences *in vitro* (49,50), its recruitment at DSBs could occur in a sequence-independent manner. In any case, whether other proteins, such as chromatin remodelers or the Ku complex, drive the localization of Rap1 at DSBs remains to be determined.

The interaction of Rap1 with Rif2 occurs exclusively *via* the Rap1^{RCT} domain (28,38,71). Structural analysis has shown that binding of both Myb-like domains around DNA constrains the orientation of the RCT domain in a conformation that may favour its interaction with the functional partners (47). By contrast, in the absence of DNA, the RCT domain can bind to Myb-C *in vitro* possibly limiting RCT interaction ability (50). Interestingly, the Rap1^{R381W} mutant variant, which increases the affinity of Myb-N to dsDNA and therefore should bind DNA with both Myb-like domains, exacerbates the DNA damage sensitivity of *rad50-VM* cells and causes telomere shortening mostly in a Rif2-dependent manner. By contrast, both P520L that decreases Myb-C affinity to dsDNA, and Y592A that impairs wrapping loop clamping, hyperactivate Rap1 mostly in a Rif2-independent manner. These findings raise the possibility that the interaction of a single Myb-like domain with DNA limits Rap1 ability to recruit Rif2 on DNA. In agreement with this hypothesis, although the amount of Rap1^{R381W}, Rap1^{P520L} and Rap1^{Y592A} bound at DSBs was increased compared to wild type Rap1, Rap1^{P520L} and Rap1^{Y592A} decreased Rif2 association to DSBs, whereas Rap1^{R381W} increased it. Altogether, these data indicate that the way Rap1 binds DNA influences its ability to interact with Rif2, with the binding of both Myb-like domains on DNA facilitating Rif2 interaction, possibly by allowing the release of the RCT from the DBD closure of the wrapping loop.

Interestingly, while Rap1^{P520L} and Rap1^{Y592A} act at DSBs and telomeres mostly in a Rif2-independent manner, they increase silencing in a Sir3-dependent manner. This finding suggests that, when Rap1 is in the conformation where only Myb-N binds to DNA, leaving Myb-C free to interact with RCT domain, the RCT domain would be less available for Rif2 binding than for Sir binding. It is worth pointing out that, while Rif2 binds to RCT in two distinct manners, involving either its N-terminal RBM motif or its C-terminal AAA+ domain, Sir3 and Sir4 proteins only bind to Rap1^{RCT} with the RBM motif. Altogether, these considerations suggest a model where RCT binding to Myb-C in Rap1 would reduce the availability of RCT interface to Rif2^{AAA+} domain, without impinging on the availability of RCT pocket for Sir3 and Sir4 and possibly Rif2^{RBM} motifs.

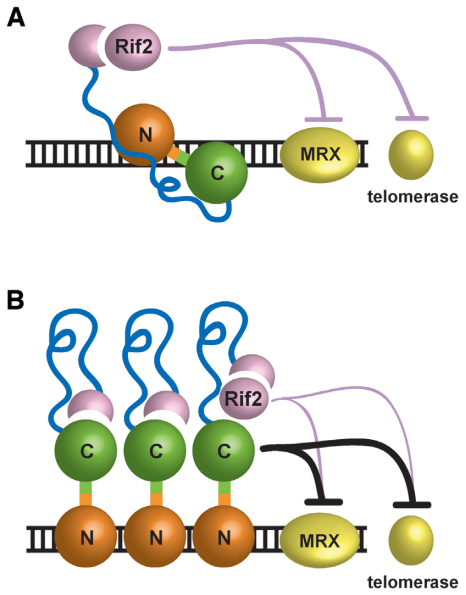

Figure 9. Model for how DNA binding modes can influence Rap1 activity in the regulation of MRX function at DSBs and of telomere length. See text for details.

We propose that binding of both Rap1 Myb-like domains to DNA allows formation of Rap1-DNA complexes that negatively regulate telomere length and MRX functions to DSBs primarily through Rif2 (Figure 9A). However, the transition to a binding mode where a single Myb-like domain is bound to DNA leads to higher stoichiometry Rap1-DNA complexes that can exert their functions on MRX association to DNA ends and telomere length in a Rif2-independent manner (Figure 9B). Interestingly, while Rap1 should bind its DNA recognition sequence preferentially with both Myb-like domains, the absence of this DNA sequence at DSBs could favour formation of Rap1-DNA complexes with high stoichiometry, where only one Myb-like domain makes contacts with DNA.

The telomeric mammalian proteins TRF1 and TRF2, as well as their fission ortholog Taz1, bind telomeric DNA through Myb-like domains (72–76). Unlike Rap1, TRF1, TRF2 and Taz1 contain a single Myb-like domain, but they bind DNA as homodimer, thus creating an overall architecture that places two Myb-like domains on DNA (42,73,77,78). Interestingly, Myb family of proteins appears to be of polyphyletic origin, implying modular evolution (79). While having two Myb-like domains in a single protein could ensure stable binding independently of the instantaneous concentration of the protein, the presence of Myb-like domains in two separate proteins could provide higher levels of regulation. In any case, the finding that Rap1 can bind DNA even through a single Myb-like domain highlights the structural plasticity of this protein and suggests

that the use of this module for DNA binding has evolved in losing one of them in mammalian proteins rather than in gaining one by yeast Rap1.

SUPPLEMENTARY DATA

Supplementary Data are available at NAR Online.

ACKNOWLEDGEMENTS

We thank J. Haber, D. Gottschling and D.P. Toczyski for yeast strains, C. Wolberger for plasmids and D. Shore for antibodies. We are also grateful to A. Johnson and A. Ronchi for technical advices on EMSA, M. Mangiagalli for Rap1 DBD purification and G. Lucchini for critical reading of the manuscript. We acknowledge Consorzio Interuniversitario del Nord-Est per il Calcolo Automatico (CINECA) for granting us the access to the high-performance computing resource MARCONI.

FUNDING

Fondazione AIRC under IG 2017 [ID 19783 to P.I. Longhese Maria Pia]; Progetti di Ricerca di Interesse Nazionale (PRIN) 2017 (to M.P.L.); Progetti di Ricerca di Interesse Nazionale (PRIN) 2017 (to D.B.); C.R. was supported by a fellowship from Italian Ministry of University and Research (MIUR) through the grant 'Dipartimenti di Eccellenza-2017'. Funding for open access charge: AIRC.
Conflict of interest statement. None declared.

REFERENCES

1. Chang,H.H.Y., Pannunzio,N.R., Adachi,N. and Lieber,M.R. (2017) Non-homologous DNA end joining and alternative pathways to double-strand break repair. *Nat. Rev. Mol. Cell Biol.*, **18**, 495–506.
2. Mehta,A. and Haber,J.E. (2014) Sources of DNA double-strand breaks and models of recombinational DNA repair. *Cold Spring Harb. Perspect. Biol.*, **6**, a016428.
3. Kowalczykowski,S.C. (2015) An overview of the molecular mechanisms of recombinational DNA repair. *Cold Spring Harb. Perspect. Biol.*, **7**, a016410.
4. Bonetti,D., Colombo,C.V., Clerici,M. and Longhese,M.P. (2018) Processing of DNA ends in the maintenance of genome stability. *Front. Genet.*, **9**, 390.
5. Gobbini,E., Cassani,C., Villa,M., Bonetti,D. and Longhese,M.P. (2016) Functions and regulation of the MRX complex at DNA double-strand breaks. *Microb. Cell*, **3**, 329–337.
6. Syed,A. and Tainer,J.A. (2018) The MRE11-RAD50-NBS1 complex conducts the orchestration of damage signaling and outcomes to stress in DNA replication and repair. *Annu. Rev. Biochem.*, **87**, 263–294.
7. Paull,T.T. and Gellert,M. (1998) The 3′ to 5′ exonuclease activity of Mre11 facilitates repair of DNA double-strand breaks. *Mol. Cell*, **1**, 969–979.
8. Trujillo,K.M., Yuan,S.S., Lee,E.Y. and Sung,P. (1998) Nuclease activities in a complex of human recombination and DNA repair factors Rad50, Mre11, and p95. *J. Biol. Chem.*, **273**, 21447–21450.
9. Cannavo,E. and Cejka,P. (2014) Sae2 promotes dsDNA endonuclease activity within Mre11–Rad50–Xrs2 to resect DNA breaks. *Nature*, **514**, 122–125.
10. Mimitou,E.P. and Symington,L.S. (2008) Sae2, Exo1 and Sgs1 collaborate in DNA double-strand break processing. *Nature*, **455**, 770–774.
11. Zhu,Z., Chung,W.H., Shim,E.Y., Lee,S.E. and Ira,G. (2008) Sgs1 helicase and two nucleases Dna2 and Exo1 resect DNA double-strand break ends. *Cell*, **134**, 981–994.
12. Shibata,A., Moiani,D., Arvai,A.S., Perry,J., Harding,S.M., Genois,M.M., Maity,R., van Rossum-Fikkert,S., Kertokalio,A., Romoli,F. *et al.* (2014) DNA double-strand break repair pathway choice is directed by distinct MRE11 nuclease activities. *Mol. Cell*, **53**, 7–18.
13. Reginato,G., Cannavo,E. and Cejka,P. (2017) Physiological protein blocks direct the Mre11-Rad50-Xrs2 and Sae2 nuclease complex to initiate DNA end resection. *Genes Dev.*, **31**, 2325–2330.
14. Wang,W., Daley,J.M., Kwon,Y., Krasner,D.S. and Sung,P. (2017) Plasticity of the Mre11–Rad50–Xrs2-Sae2 nuclease ensemble in the processing of DNA-bound obstacles. *Genes Dev.*, **31**, 2331–2336.
15. Deshpande,R.A., Williams,G.J., Limbo,O., Williams,R.S., Kuhnlein,J., Lee,J.H., Classen,S., Guenther,G., Russell,P., Tainer,J.A. *et al.* (2014) ATP-driven Rad50 conformations regulate DNA tethering, end resection, and ATM checkpoint signaling. *EMBO J.*, **33**, 482–500.
16. Cassani,C., Vertemara,J., Bassani,M., Marsella,A., Tisi,R., Zampella,G. and Longhese,M.P. (2019) The ATP-bound conformation of the Mre11-Rad50 complex is essential for Tel1/ATM activation. *Nucleic Acids Res.*, **47**, 3550–3567.
17. Ritchie,K.B. and Petes,T.D. (2000) The Mre11p/Rad50p/Xrs2p complex and the Tel1p function in a single pathway for telomere maintenance in yeast. *Genetics*, **155**, 475–479.
18. Bi,X., Wei,S.C. and Rong,Y.S. (2004) Telomere protection without a telomerase; the role of ATM and Mre11 in *Drosophila* telomere maintenance. *Curr. Biol.*, **14**, 1348–1353.
19. Larrivée,M., LeBel,C. and Wellinger,R.J. (2004) The generation of proper constitutive G-tails on yeast telomeres is dependent on the MRX complex. *Genes Dev.*, **18**, 1391–1396.
20. Chai,W., Sfeir,A.J., Hoshiyama,H., Shay,J.W. and Wright,W.E. (2006) The involvement of the Mre11/Rad50/Nbs1 complex in the generation of G-overhangs at human telomeres. *EMBO Rep.*, **7**, 225–230.
21. Nakada,D., Matsumoto,K. and Sugimoto,K. (2003) ATM-related Tel1 associates with double-strand breaks through an Xrs2-dependent mechanism. *Genes Dev.*, **17**, 1957–1962.
22. Falck,J., Coates,J. and Jackson,S.P. (2005) Conserved modes of recruitment of ATM, ATR and DNA-PKcs to sites of DNA damage. *Nature*, **434**, 605–611.
23. Lee,J.H. and Paull,T.T. (2005) ATM activation by DNA double-strand breaks through the Mre11-Rad50-Nbs1 complex. *Science*, **308**, 551–554.
24. You,Z., Chahwan,C., Bailis,J., Hunter,T. and Russell,P. (2005) ATM activation and its recruitment to damaged DNA require binding to the C terminus of Nbs1. *Mol. Cell Biol.*, **25**, 5363–5379.
25. Hirano,Y., Fukunaga,K. and Sugimoto,K. (2009). Rif1 and Rif2 inhibit localization of Tel1 to DNA ends. *Mol. Cell*, **33**, 312–322.
26. Martina,M., Clerici,M., Baldo,V., Bonetti,D., Lucchini,G. and Longhese,M.P. (2012) A balance between Tel1 and Rif2 activities regulates nucleolytic processing and elongation at telomeres. *Mol. Cell Biol.*, **32**, 1604–1617.
27. Cassani,C., Gobbini,E., Wang,W., Niu,H., Clerici,M., Sung,P. and Longhese,M.P. (2016) Tel1 and Rif2 regulate MRX function in end-tethering and repair of DNA double-strand breaks. *PLoS Biol.*, **14**, e1002387.
28. Wotton,D. and Shore,D. (1997) A novel Rap1p-interacting factor, Rif2p, cooperates with Rif1p to regulate telomere length in *Saccharomyces cerevisiae*. *Genes Dev.*, **11**, 748–760.
29. Hailemariam,S., De Bona,P., Galletto,R., Hohl,M., Petrini,J.H. and Burgers,P.M. (2019) The telomere-binding protein Rif2 and ATP-bound Rad50 have opposing roles in the activation of yeast $Tel1^{ATM}$ kinase. *J. Biol. Chem.*, **294**, 18846–18852.
30. Shi,T., Bunker,R.D., Mattarocci,S., Ribeyre,C., Faty,M., Gut,H., Scrima,A., Rass,U., Rubin,S.M., Shore,D. *et al.* (2013) Rif1 and Rif2 shape telomere function and architecture through multivalent Rap1 interactions. *Cell*, **153**, 1340–1353.
31. Azad,G.K. and Tomar,R.S. (2016) The multifunctional transcription factor Rap1: a regulator of yeast physiology. *Front. Biosci.*, **21**, 918–930.
32. Kurtz,S. and Shore,D. (1991) RAP1 protein activates and silences transcription of mating-type genes in yeast. *Genes Dev.*, **5**, 616–628.
33. Sussel,L. and Shore,D. (1991) Separation of transcriptional activation and silencing functions of the RAP1-encoded repressor/activator

protein 1: isolation of viable mutants affecting both silencing and telomere length. *Proc. Natl. Acad. Sci. U.S.A.*, **88**, 7749–7753.
34. Kyrion,G., Liu,K., Liu,C. and Lustig,A.J. (1993) RAP1 and telomere structure regulate telomere position effects in *Saccharomyces cerevisiae*. *Genes Dev.*, **7**, 1146–1159.
35. Lustig,A.J., Kurtz,S. and Shore,D. (1990) Involvement of the silencer and UAS binding protein RAP1 in regulation of telomere length. *Science*, **250**, 549–553.
36. Pardo,B. and Marcand,S. (2005) Rap1 prevents telomere fusions by nonhomologous end joining. *EMBO J.*, **24**, 3117–3127.
37. Marcand,S., Pardo,B., Gratias,A., Cahun,S. and Callebaut,I. (2008) Multiple pathways inhibit NHEJ at telomeres. *Genes Dev.*, **22**, 1153–1158.
38. Moretti,P. and Shore,D. (2001) Multiple interactions in Sir protein recruitment by Rap1p at silencers and telomeres in yeast. *Mol. Cell Biol.*, **21**, 8082–8094.
39. Kyrion,G., Boakye,K.A. and Lustig,A.J. (1992) C-terminal truncation of RAP1 results in the deregulation of telomere size, stability, and function in *Saccharomyces cerevisiae*. *Mol. Cell Biol.*, **12**, 5159–5173.
40. Liu,C., Mao,X. and Lustig,A.J. (1994) Mutational analysis defines a C-terminal tail domain of RAP1 essential for telomeric silencing in *Saccharomyces cerevisia*e. *Genetics*, **138**, 1025–1040.
41. Moretti,P., Freeman,K., Coodly,L. and Shore,D. (1994) Evidence that a complex of SIR proteins interacts with the silencer and telomere-binding protein RAP1. *Genes Dev.*, **8**, 2257–2269.
42. Li,B., Oestreich,S. and de Lange,T. (2000) Identification of human Rap1: implications for telomere evolution. *Cell*, **101**, 471–483.
43. de Lange,T. (2018) Shelterin-mediated telomere protection. *Annu. Rev. Genet.*, **52**, 223–247.
44. Graham,I.R. and Chambers,A. (1994) Use of a selection technique to identify the diversity of binding sites for the yeast RAP1 transcription factor. *Nucleic Acids Res.*, **22**, 124–130.
45. Konig,P., Giraldo,R., Chapman,L. and Rhodes,D. (1996) The crystal structure of the DNA-binding domain of yeast RAP1 in complex with telomeric DNA. *Cell*, **85**, 125–136.
46. Taylor,H.O., O'Reilly,M., Leslie,A.G. and Rhodes,D. (2000) How the multifunctional yeast Rap1p discriminates between DNA target sites: a crystallographic analysis. *J. Mol. Biol.*, **303**, 693–707.
47. Matot,B., Le Bihan,Y.V., Lescasse,R., Pérez,J., Miron,S., David,G., Castaing,B., Weber,P., Raynal,B., Zinn-Justin,S., Gasparini,S. *et al.* (2012) The orientation of the C-terminal domain of the *Saccharomyces cerevisiae* Rap1 protein is determined by its binding to DNA. *Nucleic Acids Res.*, **40**, 3197–3207.
48. Del Vescovo,V., De Sanctis,V., Bianchi,A., Shore,D., Di Mauro,E. and Negri,R. (2004) Distinct DNA elements contribute to Rap1p affinity for its binding sites. *J. Mol. Biol.* **338**, 877–893.
49. Feldmann,E.A. and Galletto,R. (2014) The DNA-binding domain of yeast Rap1 interacts with double-stranded DNA in multiple binding modes. *Biochemistry*, **53**, 7471–7483.
50. Feldmann,E.A., De Bona,P. and Galletto,R. (2015) The wrapping loop and Rap1 C-terminal (RCT) domain of yeast Rap1 modulate access to different DNA binding modes. *J. Biol. Chem.*, **290**, 11455–11466.
51. Bonetti,D., Clerici,M., Anbalagan,S., Martina,M., Lucchini,G. and Longhese,M.P. (2010) Shelterin-like proteins and Yku inhibit nucleolytic processing of *Saccharomyces cerevisiae* telomeres. *PLoS Genet.*, **6**, e1000966.
52. Vodenicharov,M.D., Laterreur,N. and Wellinger,R.J. (2010) Telomere capping in non-dividing yeast cells requires Yku and Rap1. *EMBO J.*, **29**, 3007–3019.
53. Negrini,S., Ribaud,V., Bianchi,A. and Shore,D. (2007) DNA breaks are masked by multiple Rap1 binding in yeast: implications for telomere capping and telomerase regulation. *Genes Dev.*, **21**, 292–302.
54. Iglesias,N., Redon,S., Pfeiffer,V., Dees,M., Lingner,J. and Luke,B. (2011) Subtelomeric repetitive elements determine TERRA regulation by Rap1/Rif and Rap1/Sir complexes in yeast. *EMBO Rep.*, **12**, 587–593.
55. Mangiagalli,M., Sarusi,G., Kaleda,A., Bar Dolev,M., Nardone,V., Vena,V.F., Braslavsky,I., Lotti,M. and Nardini,M. (2018) Structure of a bacterial ice binding protein with two faces of interaction with ice. *FEBS J.*, **285**, 1653–1666.
56. Abraham,M.J., Murtola,T., Schulz,R., Páll,S., Smith,J.C., Hess,B. and Lindahl,E. (2015) GROMACS: High performance molecular simulations through multi-level parallelism from laptops to supercomputers. *Software X*, **1–2**, 19–25.
57. Huang,J. and MacKerell,A.D. Jr (2013) CHARMM36 all-atom additive protein force field: validation based on comparison to NMR data. *J. Comput. Chem.*, **34**, 2135–2145.
58. Roux,B. (1995) The calculation of the potential of mean force using computer simulations. *Comput. Phys. Commun.*, **91**, 275–282.
59. Jakubec,D. and Vondrášek,J. (2019) Can all-atom molecular dynamics simulations quantitatively describe homeodomain-DNA binding equilibria? *J. Chem. Theory Comput.*, **15**, 2635–2648.
60. Deng,C., Brown,J.A., You,D. and Brown,J.M. (2005) Multiple endonucleases function to repair covalent topoisomerase I complexes in *Saccharomyces cerevisiae*. *Genetics*, **170**, 591–600.
61. Marcand,S., Gilson,E. and Shore,D. (1997) A protein-counting mechanism for telomere length regulation in yeast. *Science*, **275**, 986–990.
62. Siebenmorgen,T. and Zacharias,M. (2019) Evaluation of predicted protein-protein complexes by binding free energy simulations. *J. Chem. Theory Comput.*, **15**, 2071–2086.
63. Kirkwood,J.G. (1935) Statistical mechanics of fluid mixtures. *J. Chem. Phys.*, **3**, 300–313
64. Feeser,E.A. and Wolberger,C. (2008) Structural and functional studies of the Rap1 C-terminus reveal novel separation-of-function mutants. *J. Mol. Biol.*, **380**, 520–531.
65. Lee,S.E., Moore,J.K., Holmes,A., Umezu,K., Kolodner,R.D. and Haber,J.E. (1998) *Saccharomyces* Ku70, Mre11/Rad50 and RPA proteins regulate adaptation to G2/M arrest after DNA damage. *Cell*, **94**, 399–409.
66. Kaye,J.A., Melo,J.A., Cheung,S.K., Vaze,M.B., Haber,J.E. and Toczyski,D.P. (2004) DNA breaks promote genomic instability by impeding proper chromosome segregation. *Curr. Biol.*, **14**, 2096–2106.
67. Lobachev,K., Vitriol,E., Stemple,J., Resnick,M.A. and Bloom,K. (2004) Chromosome fragmentation after induction of a double-strand break is an active process prevented by the RMX repair complex. *Curr. Biol.*, **14**, 2107–2112.
68. Nakai,W., Westmoreland,J., Yeh,E., Bloom,K. and Resnick,M.A. (2011) Chromosome integrity at a double-strand break requires exonuclease 1 and MRX. *DNA Repair (Amst.)*, **10**, 102–110.
69. Clerici,M., Mantiero,D., Lucchini,G. and Longhese,M.P. (2005) The *Saccharomyces cerevisiae* Sae2 protein promotes resection and bridging of double strand break ends. *J. Biol. Chem.*, **280**, 38631–38638.
70. Gottschling,D.E., Aparicio,O.M., Billington,B.L. and Zakian,V.A. (1990) Position effect at *S. cerevisiae* telomeres: reversible repression of Pol II transcription. *Cell*, **63**, 751–762.
71. Liu,C. and Lustig,A.J. (1996) Genetic analysis of Rap1p/Sir3p interactions in telomeric and HML silencing in *Saccharomyces cerevisiae*. *Genetics*, **143**, 81–93.
72. Chong,L., van Steensel,B., Broccoli,D., Erdjument-Bromage,H., Hanish,J., Tempst,P. and de Lange,T. (1995) A human telomeric protein. *Science*, **270**, 1663–1667.
73. Bilaud,T., Koering,C.E., Binet-Brasselet,E., Ancelin,K., Pollice,A., Gasser,S.M. and Gilson,E. (1996) The telobox, a Myb-related telomeric DNA binding motif found in proteins from yeast, plants and human. *Nucleic Acids Res.*, **24**, 1294–1303.
74. Broccoli,D., Smogorzewska,A., Chong,L. and de Lange,T. (1997) Human telomeres contain two distinct Myb-related proteins, TRF1 and TRF2. *Nat. Genet.*, **17**, 231–235.
75. Cooper,J.P., Nimmo,E.R., Allshire,R.C. and Cech,T.R. (1997) Regulation of telomere length and function by a Myb-domain protein in fission yeast. *Nature*, **385**, 744–747.
76. König,P. and Rhodes,D. (1997) Recognition of telomeric DNA. *Trends Biochem. Sci.*, **22**, 43–47.
77. Bianchi,A., Smith,S., Chong,L., Elias,P. and de Lange,T. (1997) TRF1 is a dimer and bends telomeric DNA. *EMBO J.*, **16**, 1785–1794.
78. Bianchi,A., Stansel,R.M., Fairall,L, Griffith,J.D., Rhodes,D. and de Lange,T. (1999) TRF1 binds a bipartite telomeric site with extreme spatial flexibility. *EMBO J.*, **18**, 5735–5744.
79. Rosinski,J.A. and Atchley,W.R. (1998) Molecular evolution of the Myb family of transcription factors: evidence for polyphyletic origin. *J. Mol. Evol.*, **46**, 74–83.